Impact of sea ice cover and thickness on the regional climate model MAR simulations over the Arctic-CORDEX domain

Auteur : Lambert, Marius
Promoteur(s) : Fettweis, Xavier
Faculté : Faculté des Sciences
Diplôme : Master en sciences géographiques, orientation climatologie, à finalité approfondie
Année académique : 2017-2018
URI/URL : http://hdl.handle.net/2268.2/5588

UNIVERSITY OF LIÈGE

MASTER THESIS

Impact of sea ice cover and thickness on the regional climate model MAR simulations over the Arctic-CORDEX domain

Author:
Marius LAMBERT

Superviser:
X. FETTWEIS

Examiners:
A. DEMOULIN
L. FRANCOIS

A thesis submitted in fulfillment of the requirements
for the degree of Master in geographic sciences, climatology orientation

in the Department of Geography
Faculty of Sciences

Academic year: 2017-2018

September 2018

UNIVERSITY OF LIÈGE

Abstract

Faculty of Sciences

Department of Geography

Master in geographic sciences, climatology orientation

Impact of sea ice cover and thickness on the regional climate model MAR simulations over the Arctic-CORDEX domain

by Marius LAMBERT

Since the beginning of this century, the Arctic has experienced a rapid decrease in its sea ice extent, explaining in large part a regional climate warming (called "the Arctic Amplification") much stronger than average global warming. Sea ice concentration (SIC) and sea ice thickness (SIT) are the main factors controlling the Arctic Ocean's mean surface temperature change, by isolating upper air from warmer oceanic water. A change in surface temperature could disrupt the climate system, mainly by influencing regional atmospheric circulation.

In most regional climate models (RCMs), SIC usually comes from large-scale forcing datasets (e.g. reanalysis) and SIT is a fixed parameter as for example in the regional climate model MAR, despite its major seasonal variations. We compare here MAR simulations driven by ERA-Interim using fixed SIT to MAR simulations forced by ERA-Interim for the atmosphere and high resolution SIT and SIC from the GLORYS2V4 database, as well as by using fixed SIT but SIC from the OSTIA database. The whole set of simulations concerns the Arctic-CORDEX domain and covers years 2000 to 2015. The aim of this study is (i) to improve the representation of MAR's boundary layer over the Arctic Ocean by reducing the biases between *in situ* observations and MAR simulations over and near the Arctic Ocean and; (ii) to estimate the impact of SIC/SIT reanalysis on the Arctic boundary layer and local atmospheric circulation.

Résumé

Depuis le début de ce siècle, l'Arctique a connu une diminution rapide de son étendue de glace de mer, ce qui explique en grande partie que le réchauffement climatique régional (connu sous le nom de "Amplification Arctique") ait été deux fois plus marqué que le réchauffement moyen à l'échelle de la Terre. En jouant le rôle d'isolant entre l'océan et l'atmosphère, l'épaisseur et la concentration de glace de mer sont des éléments clés pour la régulation de la température moyenne de surface de l'Océan Arctique. Finalement, par le biais de son influence sur la circulation atmosphérique régionale, une modification de la température de surface pourrait provoquer une perturbation du système climatique.

Dans la plupart des modèles climatiques régionaux (RCMs), la concentration de glace de mer provient généralement de grilles de forçages à grande échelle (e.g. réanalyses). Tandis que l'épaisseur de glace de mer, malgré ses variations saisonnières importantes, est souvent un paramètre fixe dans les RCMs, comme c'est le cas par exemple dans le modèle atmosphérique régional MAR. Dans cette étude, on comparera des simulations du MAR forcé par ERA-intérim utilisant une épaisseur de glace de mer fixe avec des simulations forcées par ERA-intérim pour l'atmosphère mais par des réanalyses à haute résolution d'épaisseur et de concentration de glace de mer provenant de la base de données GLORYS2v4, ainsi qu'en utilisant une épaisseur de glace de mer fixe et la concentration de glace de mer provenant de la base de données OSTIA. L'ensemble des simulations concerne le domaine CORDEX-Arctique et couvre la période 2000-2015. L'objectif de ce travail est (i) d'améliorer la représentation de la couche limite atmosphérique du MAR au-dessus de l'Arctique en réduisant le biais entre les observations et les simulations au-dessus et autour de l'océan Arctique et; (ii) d'estimer l'impact des réanalyses de concentration/épaisseur de glace de mer sur la couche limite atmosphérique en Arctique et les éventuels changements de circulations locaux.

Acknowledgements

I would like first to express my deep gratitude to my superviser Prof. Xavier Fettweis. His door was always open whenever I faced an obstacle or had a question about my research. He systematically answered my emails, even late at night. I would like to thank him for his continuous support, his patience, motivation and vast knowledge. I could not have imagined having a better superviser for my master thesis.

Secondly, I wish to thank Christoph Kittel for his help especially in the interpretation of the results.

A special gratitude is due to my friend and colleague, Adrien Damseaux, for interesting and stimulating discussions about our respective subjects.

I am also grateful to Zoë Pesonen, who provided me with unfailing and continuous support and helped review the English version of my text and improve it.

Last but not least, I would like to acknowledge the support and encouragements of everyone in my circle.

…

Contents

8

List of Abbreviations

MAR	**A**tmospheric **R**egional **M**odel
SIT	**S**ea **I**ce **T**hickness
SIC	**S**ea **I**ce **C**oncentration
SIE	**S**ea **I**ce **E**xtent
SIV	**S**ea **I**ce **V**olume
SST	**S**ea **S**urface **T**emperature
NAO	**N**orthern **A**tlantic **O**scillation
AO	**A**rctic **O**scillation
AD	**A**rctic **D**ipole
SLP	**S**ea **L**evel **P**ressure
SLA	**S**ea **L**evel **A**nomaly
RCM	**R**egional **C**limate **M**odel
GCM	**G**lobal **C**ircultion **M**odel
OGCM	**O**cean **G**lobal **C**ircultion **M**odel
AOGCM	**A**tmosphere **O**cean **G**lobal **C**irculation **M**odel
CORDEX	**CO**ordinated **R**egional **D**ownscaling **EX**periment
NESTOR	**NEST**ing **O**rganization for the preparation of meteo. & surf. fields in **R**egional models
STD	**ST**andard **D**eviation
RMSE	**R**oot **M**ean **S**quare **E**rror
CRMSE	**C**entered **R**oot **M**ean **S**quare **E**rror
CEN	**C**entre d'**E**tudes de la **N**eige
FCC	**F**ederal **C**limate **C**omplex
ISD	**I**ntegrated **S**urface **D**ata
NCDC	**N**ational **C**limatic **D**ata **C**entre
LBC	**L**ateral **B**oundary **C**onditions
EOF	**E**mpirical **O**rthogonal **F**unction
UAR	**U**pper **A**ir **R**elaxation
GHG	**G**reenhouse **G**as
IR	**I**nfra**R**ed

Chapter 1

Literature review

1.1 Introduction

Climate is constantly changing: it has changed in the past, is changing now and will change in the future. The issues related to climate change are not the fluctuations of the climate itself, but rather the way in which it is changing and the underlying causes. Today, the role of human activities cannot be ignored and is more important than in the past. Humans are modifying not only the Earth's surface but also the composition of the atmosphere.

Admitting the role of humans in recent fluctuations of the climate, it is important to consider future trends. We must assess the amount of anthropogenic stress that the Earth system can handle before future changes become significant. In order to estimate that amount, the first step is to determine and understand the processes involved in the land-ocean-atmosphere-cryosphere system and their relative magnitudes. This work focuses on cryosphere-atmosphere interactions and is part of that wider context.

Future trends in sea ice thickness and sea ice cover are one of the greatest uncertainties for predicting temperature rise. This can be explained by two key processes: firstly sea ice cover (SIC) plays an important role in albedo feedback, enhancing global warming; and second, less known, sea ice thickness (SIT) insulates atmosphere from oceanic water [Schneider and Dickinson, 1974].

In recent years, there has been growing attention to Arctic Sea ice loss and its impacts on climate. However, the focus has been on sea ice extent rather than sea ice thickness despite the fact that the latter plays a key role in regulating surface heat fluxes. Until now, due to a lack of reliable data, SIT has often been kept fixed in atmospheric models. Yet along with the accelerating melt of sea ice, models with fixed thickness miss a strong source of model skill, leading to underestimation of the warming signal [Lang et al., 2017]. In addition, fixed thickness does not take into account the spatial and inter-annual variability of sea ice.

For this reason, our study focuses on the impacts of SIT on the Arctic's boundary layer, modelled by MAR. We chose the Arctic region mainly because its climate has been changing rapidly. Owing to a phenomenon called "Arctic Amplification", the warming of the past few decades has been two times stronger around the North Pole than over the whole planet on average [Screen and Simmonds, 2010].

Finally, owing to the dramatic changes in sea ice during the past 30 years, the need for efficient numerical models and high quality observational systems has grown. These tools are crucial for monitoring the state of sea ice and predicting future climate changes

that could disturb the Arctic Region and the Earth as a whole [Koldunov et al., 2010].

This Master thesis is structured as follows: Chapter 1 is a detailed state of the art description including definitions and process mechanisms related to the subject of interest. This chapter also discusses recent changes and techniques for measuring SIC, SIT and sea surface temperature (SST). Chapter 2 briefly explains the hypotheses from this research. Chapter 3 deals with the methodology, the data and the model used. The results are described in Chapter 4 and discussed in detail in Chapter 5. Finally, Chapter 6 closes the study by providing conclusions and some perspectives.

1.2 Context

Located in the northern polar region, the Arctic Ocean is the smallest and shallowest ocean on Earth. It is almost completely surrounded by Europe, Asia and North America (Figure 1.1). Partly covered by sea ice in summer and almost entirely during winter this ocean is an essential road for commerce in northern Russia. The Arctic Ocean is difficult to explore because the climate is harsh at its high latitude (mostly beyond 57 °N). In addition, sea ice can sometimes be thin at the centre of the sea ice pack and at the borders of the continents in winter. Beyond being a crucial component of the climate system, Arctic sea ice also provides a habitat for living organisms, a hunting ground for native populations and a way to travel [Koldunov et al., 2010].
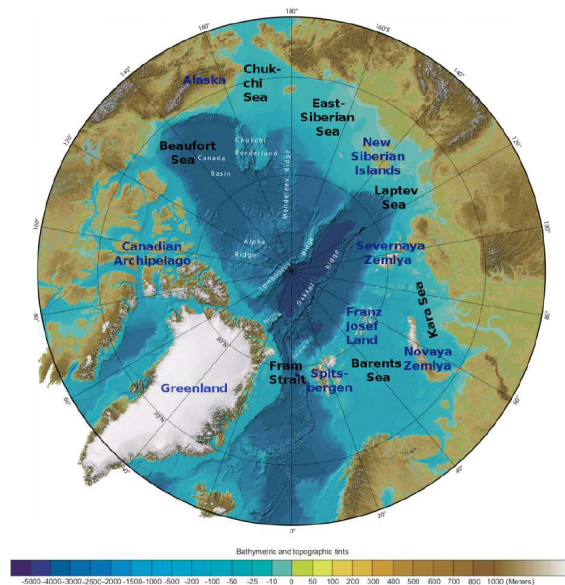
FIGURE 1.1: Arctic Ocean sea-floor features map including geographical place names. Based on a map produced by the International Bathymetric Chart of the Arctic Ocean (IBCAO). Source:[Jakobsson et al., 2008]

1.3 Recent changes over the Arctic

1.3.1 Arctic sea ice variability

Sea ice extent (SIE) is the most visible component of climate change, affecting the albedo of the Earth's surface and much more. In addition, sea ice volume (SIV) also a function of SIT, affects heat fluxes and fresh-water exchange between ocean and sea ice. According

to global climate simulations, an anthropogenic greenhouse gas forcing will contribute to a greater loss in Arctic SIV (3.4% per decade) than in SIE (2.4% per decade) [Laxon et al., 2013].

Sea ice extent

Based on Laxon et al. [2013], Arctic sea ice extent decreased during the past 30 years, with the absolute minimum observed during September 2012. Satellite records (1979-2010) show downward trends of SIE in all months, especially in winter and at the end of the melt season in September [Serreze et al., 2007b]. From 2002 onwards, Arctic sea ice extent has experienced several extreme minima in September. The first SIE minimum occurred in 2005, followed by a recovery in 2006. Later, September 2007 was marked by the lowest extent of sea ice ever recorded, falling 23% below the minimum observed in 2005 [Stroeve et al., 2008]. After the minimum of 2012, the second, third and fourth September extent minima were respectively, in 2008, 2009 and 2010. The September linear trend line shows a decrease of 13.2% per decade relative to the 1981 to 2010 average (Figure 1.2) [NSIDC, 2017].
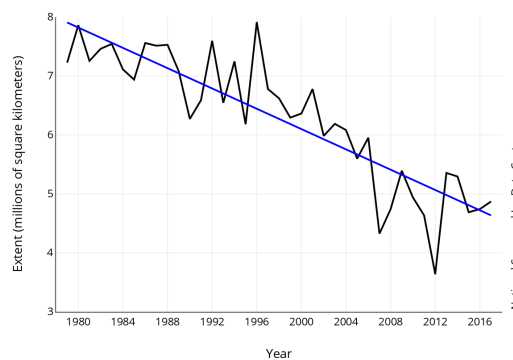
FIGURE 1.2: Evolution of mean September sea ice extent (from 1979 to 2017) with linear trend line. Source: [NSIDC, 2017]

The decreasing tendency of sea ice extent is well explained on one hand by the natural variability of air temperature as well as oceanic and atmospheric circulations, and on the other by the increase in atmospheric greenhouse gas (GHG) concentrations [Serreze et al., 2007a]. The major influence of GHG on the observed trend has been strongly proved. Nevertheless, their contribution has been underestimated, and as a result, it is clear that most simulated trends are lower than what has actually been observed. In other words, the Arctic's climate is changing faster and its mean surface temperature is increasing at a higher rate than expected by the majority of global climate models. This allows us to expect a sea-ice-free Arctic in summer before 2030 [Stroeve et al., 2007].

Even if the accelerating trend of SIE toward a seasonally ice-free Arctic Ocean is only beginning to emerge, the exponential positive response to climate forcing (amount of energy the Earth receives from the sun and radiates back into space) can be demonstrated (Figure 1.3). Less SIE and far-reaching open water areas in September lead to the presence of thin ice dominated by first-year ice (formed during the previous winter and autumn) the following spring [Stroeve et al., 2012b]. Young sea ice melts more rapidly, particularly under modified circulation patterns, as in 2007, when a SIE minimum was observed. However, the anomalous winds observed in 2007 only explain a small part of the unusual SIE of that year; the major cause was the replacement of older sea ice by first-year ice and

Global Warming year after year. The gradual change in temperature and ice replacement is called "preconditioning" and started several decades ago [Lindsay et al., 2009].

We can find two other reasons for the exponential positive response of Arctic SIE climate forcing. First, thinner ice in spring is the source of a more fragmented sea ice cover at the beginning of summer. The fragmentation would then indirectly induce the appearance of an earlier sea ice-free ocean, caused by an increase of the albedo feedback [Perovich et al., 2007]. Second, the warming of the Arctic region during all seasons will provoke an earlier melt in summer and weaken the probability of cold conditions that would bring back a recovery of sea ice in winter through natural climate variability [Stroeve et al., 2012b].
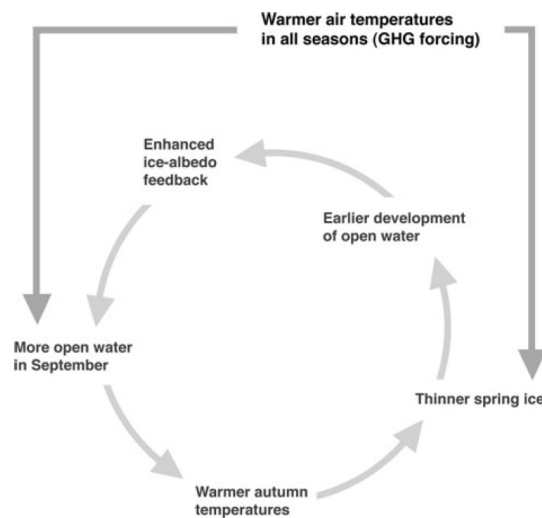
FIGURE 1.3: Processes involved in the positive feedback explaining the accelerating downward trend in Arctic SIE. Source: [Stroeve et al., 2012b]

Sea ice thickness

As SIT is a central parameter of this study, we will attach great importance to it and will go into great detail concerning its variability. Many types of variability can explain changes in SIT: seasonal variability, decadal variability, spatial variability and inter-annual variability. Each of these is described in the following sections.

Decadal variability

Numerous Arctic models have suggested changes in sea ice thickness on a decadal time-scale [Polyakov and Johnson, 2000; Chapman et al., 1994] associated with dynamic forcing. However, for some models, it remains unclear whether SIT is mainly controlled by thermodynamic forcing (thermal and radiative) or by dynamic forcing (wind stress and ocean) [Zhang and Hunke, 2001].

Decreasing trend and inter-annual variability

A study by Lindsay and Schweiger [2015] based on a combination of multiple data sources (satellites, submarines, etc...), showed a decrease of 0.58 ± 0.07 m $decade^{-1}$ in mean annual SIT over the Arctic Basin during the period 2000-2012. When the same method was applied for the period 1975-2012, SIT decreased from 3.59 m in 1975 to 1.25

m in 2012, in other words a reduction of 65% between 1975 and 2012.

Similarly, Kwok and Rothrock [2009] deduced that the mean annual SIT decreased by some 53% over 40 years by comparing submarine data (1958 to 1976) used by Rothrock et al. [1999] with satellite (ICE-sat) data (2003 to 2008). And during a shorter but more recent period, a mean decrease of 0.2 m was observed when comparing submarine data (1997 to 2003) with ICE-sat data (2003 to 2008). Before the summer retreat records of 2005 and 2007, thinning of ice occurred over a large portion of the perennially ice-covered Arctic Ocean. Retreat records have led to the replacement of old perennial ice by multilayer younger ice. Thus, since 2007, the amount of thin seasonal ice has remarkably increased, contributing to the critical overall decline of SIT [Maslanik et al., 2007; Kwok et al., 2007].

Seasonal and regional variability
The values shown in Table 1.1 represent the seasonal and regional variability of sea ice thickness over the Arctic Ocean. Koldunov et al. [2010] compared climatic observations from Romanov [1995] with two runs of the Max Planck Institute for Meteorology Hamburg Primitive Equation Ocean Model (MPI-OM). The first one (called ECHAM) corresponds to MPI-OM forced by anthropogenic forcing (CO_2, N_2O, CH_4,...), while for the second one (called FNCEP), the model is forced by the NCEP/NCAR reanalysis. The spatial distribution is poorly represented in the models, and there are significant differences between both runs. In addition, the climatic observations are highly uncertain. However, interesting information can be deduced from Table 1.1. The SIT observations for the month of April decrease continuously from the north of Greenland and the Canadian archipelago toward Alaska and the Siberian shelf (Table 1.1). In the East Siberian Sea and the north of Greenland, ECHAM shows SIT reaching 5m. Almost the same pattern is found in August/September, the only difference being that the maximum of SIT observations (3-4m) is moved toward the North Pole and decreasing in all directions. Concerning the margins of the ice shelf, SIT values of less then 70 cm were recorded at the Siberian coast and 0 cm in the Kara Sea.

Location	April			August–September		
	Atlas	ECHAM	NCEP	Atlas	ECHAM	NCEP
Central Arctic	2.4–3.2	4–4.5	2.8–4	1.8–3	3.5–4	1.8–3.3
Canadian Archipelago	3.2	4–5	4.5–5	2.8–3	4–5	4–5
Beaufort Sea	2.4–3.2	4.4	4–5	1.2–2.4	3.5–4	3.2–4
Coast of Alaska	1.8–1.2	4.5	3–4	0–0.7	0–3.2	0–2.8
Chukchi Sea	1.8–1.2	4.5–5	3.8–4	0–0.7	0–3.2	0–2.5
East Siberian Sea	1.8–2.4	4.5–5	3.5–4	0.7–1.8	3.2–3.8	2–2.5
Laptev Sea	≤1.8	3.2–3.8	2.5–3	0–1.2	2.8–3.5	1.2–2.4
Kara Sea E	1–1.7	1.8–2.8	1.5–2	0–1.2	0–1.8	0
Kara Sea W	1.3	1–2	1–1.5	0	0.7	0

TABLE 1.1: Sea ice thickness (m) for April and August–September. The label "Atlas" refers to Romanov (1995). Source: [Koldunov et al., 2010]

Figure 1.4 from Lang et al. [2017] is a result of the comparison between up-to-date information from the Global Ice-Ocean Modelling and Assimilation System (GIOMAS) and Koldunov et al. [2010]. GIOMAS is considered the best available estimate of SIT's actual long term evolution [Lang et al., 2017]. In Figure 1.4, SIT is averaged over a period of two months, October-November and February–March because according to Screen et al. [2013] a longer period would not represent its thermal response. Additionally the temperature gradient between ocean and atmosphere is stronger during winter so the most interesting period for assessing the impact of SIT ranges from October to March [Gerdes,

2006; Krinner et al., 2010].
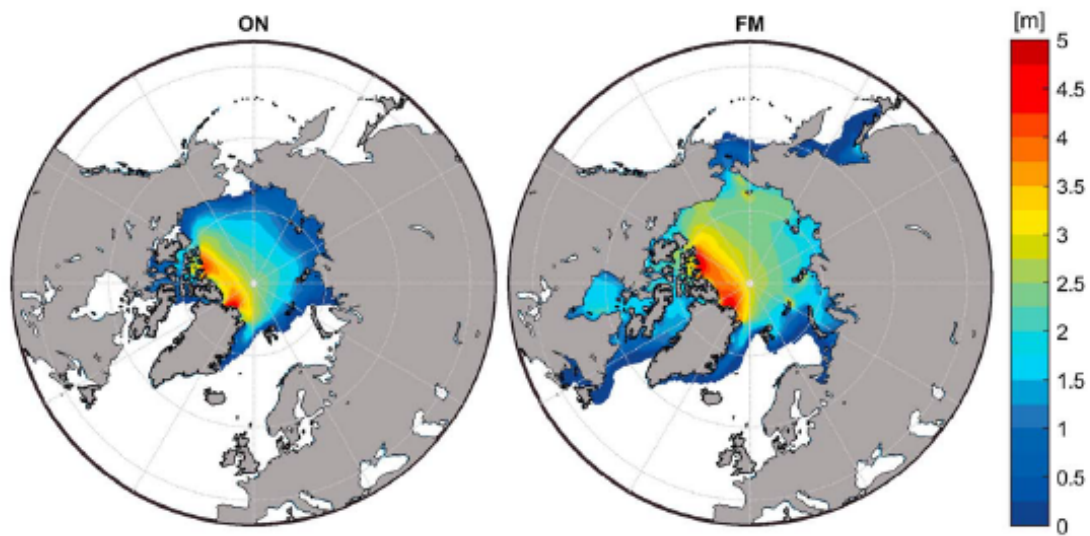
FIGURE 1.4: 1982–2013 Arctic sea ice thickness: multi-year mean for October–November (left column) and February–March (right column) according to GIOMAS. Source: [Lang et al., 2017]

1.3.2 Circulation changes and Arctic dipole

Based on Empirical Orthogonal Function (EOF) modes of SLP north of 20°, the main Arctic variability patterns are: the Arctic oscillation (AO)/North Atlantic oscillation (NAO), the Pacific North American Pattern (PNA) and the Arctic Dipole (AD) [Quadrelli and Wallace, 2004; Wang et al., 2009].

In earlier studies, the Northern Atlantic Oscillation (NAO) index was thought to be linked with Arctic sea ice retreat by Deser et al. [2000]. According to Hu et al. [2002]; Deser et al. [2000], winter sea ice would be 50 cm thinner in high-NAO index years than in low-NAO index years in Eurasian coastal regions. However, after the early 1990s, the correlation between the NAO index and sea ice disappeared because the NAO shifted while sea ice was still decreasing [Deser and Teng, 2008]. But even so, some studies still suggest that the NAO index may play a role in sea ice fluctuations [Ogi et al., 2010].

Meanwhile, a newer pattern called the Arctic dipole has been suggested to contribute to changes in sea ice over some Arctic regions [Watanabe et al., 2006]. The Arctic dipole is a persistent meridional wind pattern, beginning in 2005, and resulting from a high sea level pressure (SLP) over North America and northern Greenland and a low SLP over the Siberian Arctic (Figure 1.5) [Overland and Wang, 2010]. There are multiple impacts from this early summer wind pattern: the retreat of West Greenland's ice sheet [Rignot et al., 2011], thinner old ice and accelerated sea ice loss in summer [Kwok and Untersteiner, 2011], a possible increase in upper-level flow linking the weather of the Arctic and subarctic and positive persistent temperature anomalies [Overland et al., 2012]. According to Wang et al. [2009], the meridional flow would have been a key driver in the 2007 record of sea ice retreat.
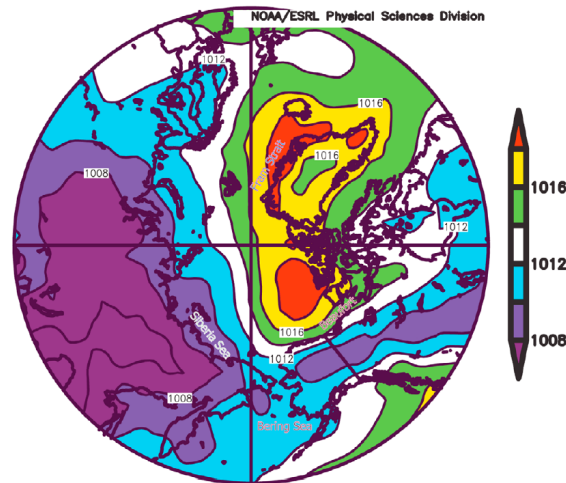
FIGURE 1.5: June sea level pressure (hPa) for 2007–2012. The data comes
from the NCEP–NCAR reanalysis. Source: [Overland et al., 2012]

Most scientists have considered AO and AD as well representing the natural variability of the North Pole's climate. But we observed that summer sea ice loss was followed by shifts in late autumn and winter large-scale atmospheric circulations. The tropospheric temperature is impacted by the increase in heat going from the ocean to the atmosphere due to thinner or non-existent sea ice in summer [Overland and Wang, 2010]. The heating of the troposphere will thus influence the geopotential height and the thickness field. In other words, along with the indices of climate variability, the feedback component of atmospheric circulation plays a key role in the recent trends of summer sea ice loss [Overland and Wang, 2010; Lang et al., 2017].

Interactions between sea ice variability and circulation changes over the Arctic are currently an area of active research [Barnes and Screen, 2015].

1.3.3 Arctic amplification and the "insulation effect"

During the past 50 years, mean surface air temperature rose twice as much over the Arctic than over the rest of the world. This phenomenon, called "Arctic amplification" is now seen as a full-fledged component of the climate system. Arctic amplification has been observed during both warm and glacial periods, but we expect the dramatic current warming to expand in the next decades [Serreze and Barry, 2011].

Many hypotheses have been suggested for the causes of this phenomenon, but sea ice loss certainly has an important part to play. The first mechanism, called "sea ice albedo feedback", is related to SIE. In summer, a dark open ocean absorbs more solar energy than an ice-covered ocean. Thus when winter comes, the excess energy caught in summer is released, warming the lower atmosphere and hence reducing winter sea ice volume. Thinner sea ice will melt more easily the following summer, increasing the absorbing open water area of the ocean [Screen and Simmonds, 2010; Döscher et al., 2014].

The second effect is the "insulation effect" [Serreze and Barry, 2011], involving SIT instead of SIE. This process is based on the insulation role of sea ice between the ocean and the atmosphere. During winter, heat spreads upward by conduction from the ocean towards the colder atmosphere. Arctic amplification is stronger in winter and autumn,

when the temperature gradient between ocean and lower atmosphere is at its highest point. SIE contributes more than SIT to Arctic amplification. In addition, other factors have been identified, including clouds, water vapour, temperature feedback and circulation changes [Lang et al., 2017]. The respective contributions of these factors are still a matter of debate. In some global climate models, water vapour and cloud cover may count more than the albedo feedback, but these models underestimate Arctic sea ice decline [Screen and Simmonds, 2010].

According to Pithan and Mauritsen [2014], the temperature feedback, rather than albedo feedback, is the main contributor to Arctic amplification. They showed that even without the positive albedo feedback, Arctic amplification was present in some models. Temperature feedback is based on the principle that when the surface heats up, more energy is emitted into space at middle latitudes than at high latitudes. This is due to:

i) the different vertical structure of warming at high and low latitudes

ii) the less important emission occurring at lower temperatures than at higher ones, for the same amount of warming.

Finally, Arctic amplification leads to changes in atmospheric circulation, vegetation and the carbon cycle and may have large-scale impacts [Serreze and Barry, 2011].

1.4   Regional climate modelling and sea ice data

1.4.1   Climate models

A climate model can be defined as a numerical representation of the planet through interactions between atmosphere, ocean and surface. To model climate, geographic space is divided into cells, each one being characterized by a different state. The more cells there are, the more precise the model will be. Mathematical and physical equations are used to represent interactions between the cells. Before starting, however, initial conditions for climate parameters (e.g. temperature and humidity) need to be fed into the model to make them evolve following the mathematical formalism [Futura, sd].

We can distinguish two types of climate models, global circulation models (GCMs) and regional climate models (RCMs). GCMs enable us to model the entire world; as a consequence, the resolution will be coarse. RCMs focus on smaller areas, allowing higher resolution and the parametrization of processes specific to the studied area. RCMs can be forced at their boundaries either by reanalyses or by GCM output datasets [Kendon et al., 2010]. However reanalyses are considered "perfect" boundary conditions, while biases in GCMs can significantly impact RCM results.

1.4.2   Reanalysis and assimilation system

A regional climate model has to be forced at each time step, meaning that we have to impose a state for the climate (temperature, wind,...) at its boundaries. The most common way to proceed is to use reanalysis, as it estimates well the observations. Reanalysis is a scientific method providing information on how the Earth's weather and climate have been changing over time since 1850. The results are generated using different meteorological data sources (satellites, meteorological stations, buoys,...), which are assimilated and modeled with a numerical climate prediction model. The final product is a synthesized representation of the whole system's state, from the Earth's surface to layers above

the stratosphere and extending over several decades. It contains realistic estimates of atmospheric variables at several levels and surface variables such as rainfall, soil moisture, SST. Reanalysis is mostly used in climate research for monitoring climate conditions and preparing predictions, but it is also increasingly used in other sectors such as agriculture, energy and water resources. It is clear that the quality of the reanalysis varies spatially, being more accurate in regions where more data are assimilated [Reanalyses.org, 2010].

Much reanalyses are open source and can be found easily on the internet. The ECMWF, National Aeronautics and Space Administration (NASA), National Centers for Environmental Prediction (NCEP) and National Oceanic and Atmospheric Administration (NOAA) are major organisations in reanalysis development, and together provide a wide range of atmospheric and oceanic reanalyses. Each reanalysis is characterized by a specific period, resolution and time-step. The assimilation method and system or employed model are essential features to build upon when selecting reanalyses [Dee et al., 2016]. Only three are used in this study (see Table 2.1 in Chapter 2).

1.4.3 Cordex

Since the beginning of this century, various regionalization techniques (also called downscaling techniques) have been developed. Their aim is a spatial refining of ocean-atmosphere coupled GCM (AOGCM) climate information. Until recently, AOGCMs were the major source of regional climate information, although their resolution is coarse and does not allow an accurate description of local scale projections and extreme events [Giorgi et al., 2001].

Downscaling techniques have been divided into two classes, dynamical downscaling (DD) and statistical downscaling (SD). Dynamical downscaling uses RCMs driven by reanalyses or GCM outputs [Rockel, 2015; Wang et al., 2004]. In contrast, statistical downscaling relies on statistical relationships for the prediction of regional to local-scale climate variables (predictands) from large-scale variables (predictors) [Benestad et al., 2008].

Regional climate downscaling (RCD) studies, encompassing both DD and SD, have often been conducted independently of each other. In other words, each of them responded to specific interests, resulting in underutilization of their products for climate change assessments. Giorgi et al. [2009] believe this may be due to the lack of a coordinated framework to asses RCD techniques.

Born of the need for climate change information at a regional instead of global scale, the Coordinated Regional Climate Downscaling Experiment (CORDEX) is a double framework initiated in 2009 by the World Climate Research Program (WCRP). Its first objective, part of the model "evaluate framework", is to provide a structure to evaluate and benchmark model performance. The second is to design a set of experiments for the production of climate projections, called the climate "projection framework". Behind these two objectives, the goal is to make these frameworks accessible to a large, world-wide scientific community [Giorgi et al., 2009]. CORDEX has defined some integration domains distributed all over the world, 13 in total by 2015.

This study is part of the CORDEX experiment, as our simulations are on the Arctic-CORDEX domain.

1.4.4 Data record

Reanalyses, based on spatial observations, are used to force models at their boundaries. This section describes how we measured the variables used to elaborate reanalyses or force GCMs. We focused on SST, SIT and SIC, as these three variables are the only ones used to force our model at the oceanic surface into its integration domain. Moreover, these variables are essential for assessing climate predictions.

Sea ice thickness data records

The lack of large-scale, continuous SIT measurements means that simulations of numerical Arctic models remain untested. In other words, many simulations could not be validated by comparing their results with observations [Steele and Flato, 2000]. However, in recent years the scientific community has developed a great interest in Arctic sea ice as the volume of ice is dramatically decreasing. Data and information concerning thickness of sea ice have become more consistent over the past few years [Lindsay and Schweiger, 2015].

During the past decades several ways to measure SIT have been developed by the scientific community. Historically drill holes or electromagnetic ground based methods were commonly used. These methods require a large amount of samples and are difficult to extrapolate because the snow pack is very heterogeneous at some places [Lindsay and Schweiger, 2015].

Since 1958, upward-looking sonars (ULSs) mounted on submarines are also retrieving SIT observations. These datasets are the longest records available today, some of them covering from 1975 until 2005. Unfortunately, the sampling is sparse and is limited concerning seasonal variations [Lindsay and Schweiger, 2015]. Since the Science Ice Expeditions (SCICEX) effort [Edwards and Coakley, 2003] in 1993 (a program aiming to study the Arctic Ocean), there have been few submarine cruises [Rothrock et al., 1999, 2008]. Similarly, many groups have used ULSs, but fixed on moorings instead of submarines. Their temporal sampling is excellent, and moreover, some cover an expanded period of 10 years [Rothrock et al., 1999, 2008].

Since 2001, helicopters equipped with electromagnetic sensors have been used to measure sea ice and snow thickness [Pfaffling et al., 2007]. And in 2009, operation ICEbridge used lidar and radar on a fixed-wing aircraft [Kurtz et al., 2012].

Concerning lidar satellite data retrieval, ICEsat first recorded SIT for the period 2003-2008 [Kwok and Rothrock, 2009]. Radar altimeter satellite's first data records were made by Envisat (2002-2012) [Peacock and Laxon, 2004] and later Cryosat-2 (2010) [Laxon et al., 2013].

Sea ice extent

SIE is not monitored directly. In fact, SIC retrieved from satellite sensors is used to calculate SIE, which is defined as areas with more then 15% of SIC [Parkinson et al., 1999]. The first sources of global SIE coverage became available in 1966 with satellite visible and infrared (IR) imagery. Prior to that, ships, buoys and aerial observations were the only available ways to measure SIE. Unfortunately, they expanded over a limited period of time, were not global and did not cover the whole year [Vinnikov et al., 1999]. In 1972, three passive microwave satellites were launched, but their data was poor and filled with

gaps or did not cover polar regions [Ferraro et al., 1996].

SIE has been retrieved continuously at high resolution since the beginning of the satellite era in 1979 [Lang et al., 2017], using passive microwave sensors [Stroeve et al., 2012a]. Firstly, the Scanning multichannel microwave radiometer (SSMR) was launched on NASA's Nimbus 7 satellite (from 1979 to 1987). Then the Defense Meteorological Satellite Program (DMSP) employed the Special Sensor Microwave/Imager (SSMI) (from 1987 to 2007) and later the Special Sensor Microwave Imager/Sounder (SSMIS) (from 2008 to the present) [Ferraro et al., 1996; Cavalieri et al., 1999; Stroeve et al., 2012a]. These instruments measure the thermal radiation emitted by the Earth's surface and atmosphere for four frequencies between 19 and 85 GHz [Ferraro et al., 1996].

Along with these sensors, in 2002, the Advanced Microwave Scanning Radiometer (AMSR-E), launched on EOS-Aqua satellite, was a major step because it has a wider swath, a wider spectral range and a higher resolution than passive-microwave imagery [Comiso et al., 2008; Comiso and Nishio, 2008].

Sea surface temperature

SST records go back to the 1880s, when SST was traditionally measured from ships or drifting buoys. The data were scarce in some regions and presented limited spatial coverage [Rayner et al., 2006]. Since 1981, wide swath IR instruments, for example, Advanced Very High Resolution Radiometer (AVHRR), have been used to deliver daily SST with global coverage. From 1991 to the present, Along Track Scanning Radiometer (ATSR) and other multi-channel instruments have used a more accurate along-track scanning method called "dual-view". This approach allows atmospheric corrections but the swath coverage is reduced to 512 km, so that one month is needed to obtain global coverage. Another option is to use the SEVIRI (Spinning Enhanced Visible and Infrared Imager) instrument, which allows an output every 15 minutes with a resolution of 5km but with a reduced accuracy [Donlon et al., 2012; O'Carroll et al., 2006]. IR radiometers on spacecraft are a widely used source of SST spatial observations because of their high accuracy and resolution (1-4 km) [Gentemann et al., 2010].

Prior to 1997, only IR radiometers were employed to measure SST, but with the development of the Tropical Microwave Imager (TMI), microwave retrievals became available. Since then, many other microwave instruments have been launched: Advanced Microwave Sounding Radiometer (AMSR-E), Windsat, GMI, AMSR2 [Donlon et al., 2012; O'Carroll et al., 2006]. The microwave retrievals have the advantage of not being blocked by clouds, unlike IR measures, but both are impossible when it rains, in regions with sun glitter or close to land [O'Carroll et al., 2006]. As for water vapour, wind speed and rain, the frequencies used to measure SST range between 4 and 11 GHz [Gentemann et al., 2010].

1.5 Sea ice thickness and heat fluxes

The thickness of Arctic perennial sea ice is close to 3 m [Rothrock et al., 2008], while that of seasonal sea ice is approximately 0.5 m, according to Worby et al. [2008]. As perennial sea ice has been slowly replaced by seasonal sea ice since the beginning of this century, we can foresee that before the end of the twenty-first century, Arctic sea ice will be essentially seasonal and therefore thinner than it is today [Krinner et al., 2010].

Even the most extreme climate predictions still suggest the presence of sea ice over the Arctic Ocean in winter. Therefore, the thinning of sea ice will have considerable impacts on the Arctic's climate during cold seasons. While in summer, the SIT is not important relative to the decrease of SIE as the temperature gradient between surface air (close to 0°C) and oceanic water is weak.

In winter, the ocean's surface gains energy mainly through downward IR radiation, latent and sensible heat fluxes and oceanic heat conducted through sea ice. If we suppose a 10 cm thickness of sea ice along with -40°C at the surface, we obtain a flux of 70 W/m^2. It is not negligible when compared to the surface's main source of energy loss, the thermal radiation (± 160 W/m^2). In contrast, if sea ice was 3 m thick, we would get an upward conduction flux of 25 W/m^2. The difference between both situations is not negligible within the total surface energy budget [Krinner et al., 2010].

The impacts of sea ice thickness on climate predictions have received little attention compared with the impacts of sea ice extent. Probably due to a lack of comprehensive SIT data until now, this variable is often kept fixed in atmospheric-only models. Not taking SIT into account is a significant loss of model skill because the surface temperature may be underestimated owing to sea ice thinning [Lang et al., 2017]. In addition, SIT changes can induce atmospheric changes of almost the same magnitude as those resulting from SIC changes [Gerdes, 2006]. However, some earlier studies [Krinner et al., 2010; Rinke et al., 2006; Lang et al., 2017; Gerdes, 2006] had already analysed the influence of sea ice thickness on atmospheric conditions.

Rinke et al. [2006] forced a regional atmospheric model with the SIT from an oceanic model and compared the results with their model forced by the constant SIT of 2 m. It is very similar to what is done in this study. They showed evidence that surface temperature was driven by the imposed thickness and that the major influence took place at marginal areas of ice floe. The maximum heat transfer takes place at the edges of sea ice and at the beginning or at the end of winter, when sea ice is thin and snow cover is poor [Krinner et al., 2010]. In addition, some atmospheric circulation changes were observed over the whole Arctic Ocean [Rinke et al., 2006].

Similarly, Lang et al. [2017] forced a global atmospheric model (EC-earth) with SIT from the assimilation system GIOMAS and compared it with the control run of 1.5 m fixed SIT. Based on their study, an increase of 1°C per decade due to SIT decrease is predicted in marginal sea ice areas but high internal variability would prevent local anomalies from influencing middle latitudes via the atmospheric circulation.

1.6   Motivation and objectives

In order to improve predictions of future atmospheric conditions over the Arctic and its surroundings in the global warming context, it is crucial to better understand the influence of sea ice thinning. This is the reason we chose to simulate the Arctic's climate under various SIT conditions. For this purpose, we used a regional climate model (RCM) instead of a global climate model (GCM) since GCMs have a coarser horizontal resolution and simplified physics for representing surface processes. We selected the Modèle Atmosphérique Régional (MAR) to carry out this research, as it was initially developed for studying polar regions. The results communicated by Akperov et al. [2016] also highly motivated this study, as they identified MAR as one of the worst RCMs used

in the CORDEX-Arctic experiment for estimating cyclone frequency and depth over Arctic. Since cyclone development depends on the conditions in the atmospheric boundary layer, we deduced that these conditions were not well represented in the Arctic for MAR simulations. Since that study, MAR has evolved and a new version has been created. However, knowing the insulation effect of sea ice, we expect that implementing time varying SIT into MAR could further improve its performance. Although SIT is an essential variable in climatic physical processes, MAR's current version is driven by SIC and SST but SIT is kept fixed (50 cm).

The first goal of this study was to improve the representation of MAR's boundary layer over the Arctic Ocean by reducing the biases between *in situ* observations and MAR simulations. The second goal, closely linked to the first, was to asses the added value of high resolution time and spatial varying SIT data implemented into MAR. In other words, we wanted to know whether MAR simulations significantly change the simulated state of the Arctic boundary layer when taking SIT into account. In the same vein, we estimated the impact of SIC and SST datasets on MAR simulations over the Arctic Ocean by keeping unchanged the ERA-interim based lateral forcing. To do so, MAR was forced by different reanalyses. Finally, we wanted to estimate the influence of SIC,SST and SIT on the Arctic's local atmospheric circulation changes.

Arising from the previous aims, we wanted to determine whether a coupling between MAR and an oceanic model (e.g. NEMO) would be useful for improving MAR simulations. This coupling induces the outputs of the oceanic model to be directly used as a forcing to the MAR instead of the ERA-interim reanalysis. Constraining MAR with an oceanic model has two benefits; first, the resolution of the input data is higher, and second, it will yield additional information on SIT which is not provided by ERA-interim. We considered in this study that the coupling could be judged useful if the anomaly of the skin temperature between simulations using time and spatial varying SIT and simulations with fixed SIT were significant.

Chapter 2

Data and Methodology

2.1 Data

In Chapter 1, historical and technical aspects of SIT, SST and SIC measurements were presented in a broad sense. In contrast, here more information is given on the sources of the measurements specifically used in this study. This chapter also provides more information about *in situ* observations from NOAA and ECAD that were used to evaluate our model simulations. The latter observations (from ECA&D and NOAA) include precipitation, sea level pressure and near-surface temperature.

2.1.1 Reanalyses

This study employed three sources of reanalyses, summarized in Table 2.1. They are linked, as ERA-interim uses outputs from OSTIA and GLORYS is based on atmospheric conditions provided by ERA-interim.

REANALYSIS	SOURCE	RESOLUTION	TYPE	PERIOD	REFERENCE
ERA-interim	ECMWF	0.75°x 0.75°	Atmospheric	1979-2017	Dee et al. [2011]
OSTIA	NCOF	0.05°x 0.05°	Oceanic	1985-2017	Donlon et al. [2012]
GLORYS2v4	CMEMS / Mercator ocean	0.25°x 0.25°	Oceanic	1993-2015	Garric et al. [2017]

TABLE 2.1: Description of the reanalyses used in this study. ECMWF (European Centre for Medium-Range Weather Forecasts), NCOF (The national centre for ocean forecasting) and CMEMS (Copernicus marine environment monitoring service).

ERA-interim

The ECMWF project to build the ERA-interim reanalysis was initiated in 2006 to replace the ERA-40 reanalysis. The main objectives were to resolve some assimilation difficulties encountered during the production of ERA-40 and to improve the technical aspects as many as possible. The aspects include the quality control, data selection and bias correction, as well as the representation of the hydrological cycle and the quality of the stratospheric circulation.

The gridded data from ERA-interim provides 3-hourly surface parameters and ocean wave and land surface conditions, along with 6-hourly upper air parameters, over a period ranging from 1979 to the present. The reanalysis initially started in 1989, but in 2011 the period was extended to 1979 [Berrisford et al., 2011].

The ECMWF's assimilation system used to produce ERA-interim is based on the cycle 31r2 of the Integrated Forecast System (IFS), which was released in 2006. The model uses the 12-hourly four-dimensional variational analysis of the upper-air atmospheric state [Dee et al., 2011]. This core component is an improvement in atmosphere analysis since ERA-40 used a 3D-var analysis scheme [Courtier et al., 1998]. The spatial resolution is $\pm$ 79 km (T255 spectral) and there are 60 vertical levels between the surface and 0.1 hPa [Dee, 2014].

Satellite retrievals provide most of the assimilated data, and their proportions increase with time. The main parameters involved are: brightness, temperature, ozone profiles, wind, precipitable water vapour and atmospheric motion vectors. *In situ* observations, of temperature, wind and specific humidity are present as well. Provided by radiosondes, balloons, aircraft and wind profilers (increasingly since 1998, except for aircraft observations), these *in situ* measurements have been constant since the beginning of the ERA-interim period. Meteorological land stations, ships and buoys, are another source of *in situ* observations of surface pressure, 10 m wind, 2 m temperature and relative humidity. More details concerning all these inputs are found in Dee et al. [2011]. However, it is interesting to note that since 2009, SST and SIC used to prescribe the ERA-interim model are provided by OSTIA (NCEP was used before 2009).

OSTIA

To study the influence of high-resolution SST and SIC reanalyses on MAR simulations, we used products from the Operational Sea Surface Temperature and sea-Ice Analysis (OSTIA) system. OSTIA was developed by the Met Office and provides daily SST and sea ice data at a resolution of 1/20° for the period from 1985 to near real time.

OSTIA uses satellite IR and microwave data in combination with *in situ* measurements. SST data is provided by multiple agencies through the Group for High Resolution SST (GHRSST) and via the Global Telecommunications System (GTS). For SIC, data are produced by the EUMETSAT Ocean and Sea Ice Satellite Applications Facility (OSI-SAF). All satellite SST data are bias corrected based on both ENVISAT AATSR and data from drifting buoys. Data are filtered using the surface wind speed to remove diurnal variability and an adjustment is needed to get AATSR SST measurements at the same depth as drifting buoys SST observations. The final products are not tainted by a mean bias and are characterized by an accuracy of $\pm$ 0.57 K compared to *in situ* data [Donlon et al., 2012; Stark et al., 2007].

The OSTIA reanalyses have a cold bias of 0.10 Kelvin with respect to independent Argo data. The high resolution (1/20°) daily OSTIA reanalysis climatology is available through MyOcean project (http://www.myocean.eu.org) [Roberts-Jones et al., 2012].

Glorys2v4

The outputs, produced by numerical oceanic circulation models, are combined with satellite records and *in situ* observations in order to generate an estimation of the ocean's state: sea ice thickness, salinity, temperature...

The MyOcean Global Monitoring and Forecasting Centre (CMEMS) has produced eddy permitting global ocean reanalysis (at 1/4°) for the period 1993 to 2015. Altimeter data were used from multiple satellites beginning with ERS-1 and Topex-Poseidon in the early nineties. Many daily products, such as sea surface height, salinity and sea ice velocity, are provided in Netcdf format.

The reanalysis system GLORYS2v4 is based on NEMO 3.1 (Nucleus for European Models of the Ocean), which is a global oceanic circulation model (OGCM). NEMO is configured with a tripolar ORCA grid type at 1/4°, and it's vertical grid has 75 z levels. NEMO's surface is driven by the ERA-interim reanalysis from the ECMWF. The simulations begin on the fourth of December 1991, and after the first two weeks, the time-step stabilizes at 1440 seconds.

The data were assimilated into the reanalysis system using a modified form of reduced Kalman filter called SEEK (Singular Extended Evolutive Kalman) together with a bias correction. The Kalman filter is an algorithm that estimates unknown variables from a series of measurements. It works in two steps: first, current state variables are estimated from the previous state estimations. Next, a correction is applied to the current state estimates, giving the most accurate ones a higher magnitude. This allows the removal of some errors, including noise.

The assimilated observations were sea level anomaly (SLA), SST, SIC and *in situ* profiles of temperature and salinity. As assimilation of SLA required mean sea surface height, an adjustment of the mean dynamic topography (MDT) dataset (MDT-CNES_CLS13) was used instead. Regarding SIC, the data were an IFREMER/CERSAT product, and CERSAT (ERS Processing and Archiving Facility) is part of the ESA (European Space Agency). Temperature and salinity profiles were taken from the Coriolis Ocean dataset for ReAnalysis (CORA 4.1) and AVHRR-only-SST at 1/4°from NOAA.

2.1.2   Meteorological *in situ* observations.

To calibrate and evaluate the model, the stations providing observations were selected from two databases (NOAA and ECA&D). Their choice was based on two criteria, the first, a sparse sampling for catching the spatial uncertainties, and the second, the minimization of missing values in the precipitation, near-surface temperature and sea level pressure datasets.

NOAA observations

The data summaries provided by NOAA's National Climatic Data Centre (NCDC) are based on data exchanged under the World Weather Watch program, according to the World Meteorological Organisation (WMO) Resolution 40 [W.M.O., 2016; Nael, 2006]. The NCDC produces daily datasets on the basis of hourly and synoptic observations from the U.S. Air Force DATSAV3 Surface Data and the Federal Climate Complex (FCC) Integrated Surface Data (ISD). The ISD project was initiated in 1998 by the NCDC with the goal to provide a uniform collection of hourly and daily datasets. The most important

Database	Station	Country	Weather station			Associated MAR pixel		
			Latitude	Longitude	Altitude (m)	Latitude	Longitude	Altitude (m)
ECA&D	Angisoq	Greenland	59.98	-45.13	20	60.17	-45.00	154
	Daneborg	Greenland	74.30	-20.22	44	74.31	-19.98	96
	Hopen Island	Norway	76.50	25.07	6	77.36	22.93	125
	Reykjavik	Iceland	64.13	-21.90	52	63.83	-21.80	26
	Tasiilaq	Greenland	65.60	-37.63	50	65.72	-38.33	320
NOAA	Angisoq	Greenland	59.98	-45.20	16	60.16	-43.81	506
	Angoon	United States	57.50	-134.59	0	57.51	-134.50	158
	Daneborg	Greenland	74.30	-20.22	44	74.31	-19.98	96
	Hopen Island	Norway	76.50	25.07	10	77.36	22.93	125
	Kivalina Airport	United states	67.73	-164.55	3	67.92	-164.80	71
	Kotlas	Russia	61.23	46.72	56	61.35	46.25	122
	Ougolny Airport	Russia	64.73	177.74	59	64.77	178.00	111
	Taloyoak	Canada	69.55	-93.58	28	69.46	-93.73	28
	Thule Air Base	Greenland	76.53	-68.70	76	76.54	-68.55	210
	Tiksi	Russia	71.70	128.90	9	71.62	129.10	72

TABLE 2.2: Information on the stations from the European Climate Assessment & dataset (ECA&D) and the National Oceanic and Atmospheric Administration (NOAA) used to evaluate the MAR simulations. The associated longitude and latitude are given for the centre of the MAR pixels and the height is an average on its surface. (Latitude and longitude in decimal degrees)(Grey boxes indicate stations that are taken from both sources [ECA&D and NOAA])

being: the Automated Surface Observing System (ASOS), Automated Weather Observing System (AWOS), Meteorological Airport Report (METAR) and Coastal Marine Automated Network (CMAN) [Smith et al., 2011].

Since 2003, the data processing of the FCC includes a quality control check of the observations in order to eliminate random errors. The quality control is done through several verifications: a validity check, an extreme value check, an internal consistency check (within the observations) and an external check (with observations from other stations) [Lott and Baldwin, 2001]. Nevertheless, the datasets contain missing values flagged with "9999.9" or "99.99", depending on parameters.

In 2011, more than 20000 stations with archives from 1900 to the present were involved in the ISD project. This corresponds to a total data volume of 500 GB [Smith et al., 2011]. Concerning the daily time series, 18 surface elements (including sea level pressure, near-surface temperature, precipitation, wind speed, visibility and snow depth) from over 9000 stations were available in 2006, some going back to 1929 but most from 1973 to the present [Nael, 2006].

In this study, the daily datasets used from NOAA (www7.ncdc.noaa.gov/CDO/cdo) were limited to sea level pressure, precipitation and near-surface temperature from 10 stations (Angisoq, Ougolny Airport, Angoon, Daneborg, Hopen Island, Kivalina Airport, Kotlas, Taloyoak, Thule Air Base and Tiksi) over the period 2009-2011 (Table 2.2 and Figure 2.1).
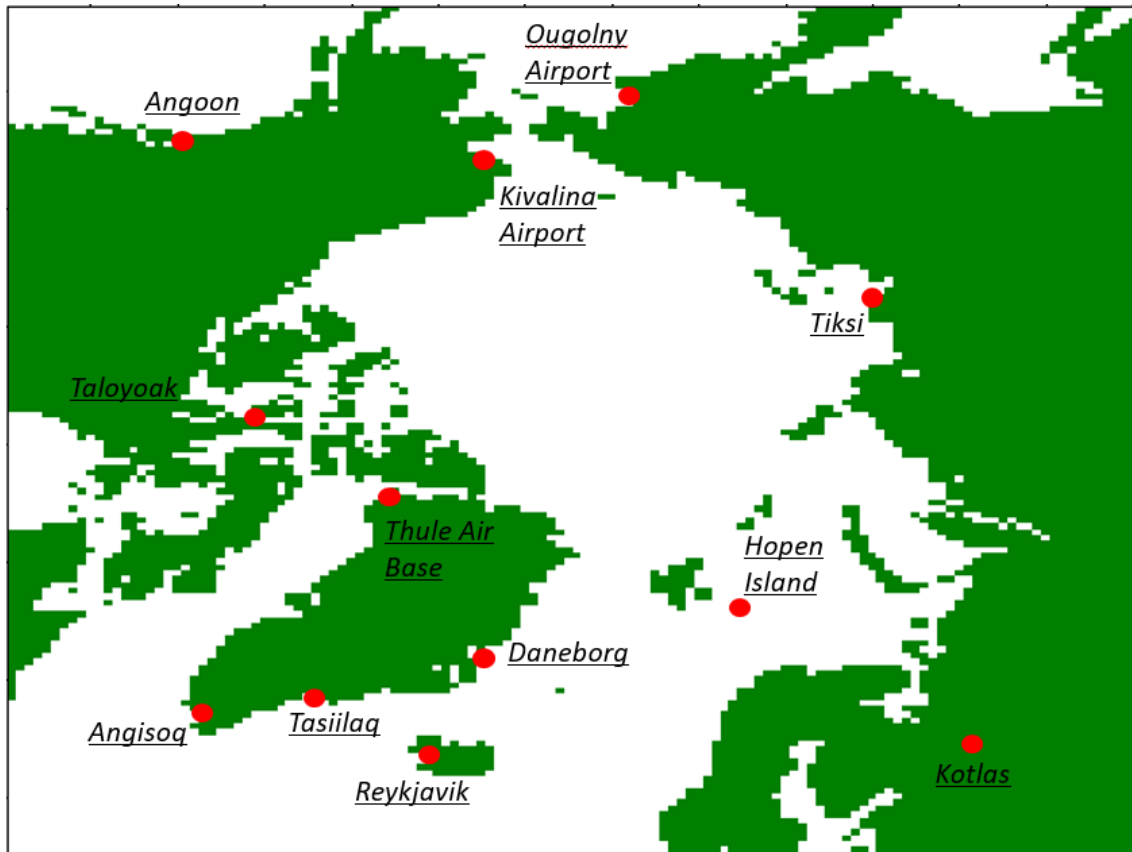
FIGURE 2.1: Location of the European Climate Assessment & Dataset (ECA&D) and National Oceanic and Atmospheric Administration (NOAA) stations used for the evaluation of the MAR simulations. (land is represented in green)

ECAD observations

ECA&D is an online database of daily meteorological observations initiated by the European Climate Support Network (ECSN) and coordinated by the Royal Netherlands Meteorological Institute (KNMI), which also funds the project. Aiming to make data publicly available, ECA&D started as a collaboration among meteorological institutes and universities throughout Europe and the Middle East (Lebanon, Israel, Syria and Jordan). Another of its objectives is to apply uniform analysis methodologies to the monitored observation series for as many stations as possible [Klein Tank et al., 2002].

Some time-series contain missing observation days, suspicious (non-climatic) jumps or gradual shifts due to changes of instruments, measurement practices or displacement of the station. For this purpose, ECA&D also ensures basic quality control and homogeneity checks. These verifications allow the identification of the number of days with uncorrectable mistakes and their flagging with "missing values" [Klok and Klein Tank, 2009]. After the quality control, the time-series are blended with those from surrounding stations and the global telecommunication system (GTS) to create long time-series used to calculate the ECA&D indices of extremes and the E-OBS daily gridded observational dataset [Hofstra et al., 2009; Haylock et al., 2008].

In 2001, 114 temperature series and 118 precipitation series were available. At that

time a comparison between ECA&D datasets and gridded datasets of monthly resolution showed a correlation above 0.8 for 93% of the near-surface temperature series and of 53% for the precipitation series over the period 1946-1999 [Klein Tank et al., 2002]. In 2013, ECA&D contained data from more than 7500 stations and 12 elements including precipitation, mean near-surface temperature, sea level pressure, sunshine duration and snow depth. The database is still expanding and is updated every month [Klok and Klein Tank, 2009].

For the evaluation of the simulations of this study, we used ECA&D's non-blended daily datasets of precipitation, near-surface temperature and sea level pressure for 2009 until 2011 from five stations: Angisoq, Daneborg, Hopen Island, Reykjavik and Tassilaq (WWW.ECAD.eu) (see Table 2.2 and figure 2.1).

2.1.3   Treatment of *in situ* observations

The retrieved observations were characterized by many missing values, especially for precipitation. Those missing values were not taken into account for the calculation of statistics. Unrealistic data were verified in this study even if quality control has already been done by the source agencies (NCDC/ECA&D). In addition, in order to be commensurate, the units of the datasets were standardized to °C for near-surface temperature, hPa for sea level pressure and mm for precipitation.

2.2   Regional atmosphere model (MAR)

2.2.1   Model overview

The model used was the RCM called MAR. After its creation in 1990, it was developed first at the University of Louvain-La-Neuve and later simultaneously at the IGE (Environment Geoscience Institute) and University of Liège. Even though it has been used to simulate the climate of several regions (Belgium [Wyard et al., 2015], inter-tropical Africa [Doutreloup et al., 2017], Antarctica [Amory, 2016], Svalbard [Lang, 2012] and Greenland [Fettweis et al., 2017]) it specializes in polar regions. It is able to simulate realistic air/snow interactions and wind over ice sheets and is probably best known for its reliable calculation of Greenland's surface mass balance over the present climate [Vernon et al., 2013; Rae et al., 2012; Navari et al., 2016].

MAR is composed of a 3D atmospheric module coupled with a 1D transfer scheme between soil and atmosphere (Soil Ice Snow Vegetation Atmosphere Transfer or SISVAT) (Figure 2.2). The atmospheric part of the MAR is described by Gallée and Schayes [1994]; Gallée [1995], while a description of SISVAT can be found in De Ridder and Gallée [1998]; Gallée et al. [2001]. The snow-ice part of SISVAT was inspired by a snow model called CROCUS [Brun et al., 1992], and developed at the CEN (Centre d'Etudes de la Neige).

CROCUS is a multilayer energy balance model that takes into account the interactions between sea ice, the ice cap and tundra on the one hand and the atmosphere on the other. The model also takes into account refreezing of meltwater and snow metamorphism, which influence surface albedo and the transformation of snow into ice.

2.2.2 MAR description

MAR solves the atmospheric primitive equations employing both the hydrostatic equilibrium and the continuity equation. The vertical coordinate is given by the the normalized pressure (σ):

$$\sigma = \frac{p - p_t}{p_s - p_t}$$

Where p is the pressure at a considered point, p_t the constant pressure at the top of the model and p_s the surface pressure.
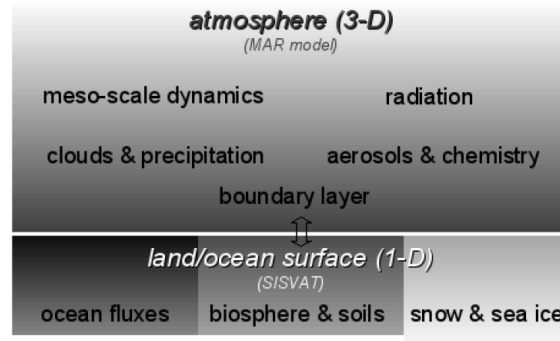
FIGURE 2.2: General description of MAR. Source: [Fettweis, 2006]

MAR includes a solar radiative scheme from Fouquart and Bonnel [1980]. While the long-wave radiation scheme is that of Morcrette [2002], and underestimation of solar incoming radiation was corrected by Fettweis [2006]. The resolution of the hydrological cycle was carried out by a micro-physical cloud model with conservation equations for cloud particles (raindrops, droplets, ice crystals, snowflakes) [Gallée, 1995]. Also, the parametrization of convection is based on the mass-flux convection scheme of Bechtold et al. [2001]. Finally, the parametrisation of the vertical fluxes near the planetary boundary layer is based on the $E - \epsilon$ turbulence closure model of Duynkerke [1988].

2.2.3 SISVAT description

The SISVAT vertical multilayer model calculates the interactions between atmosphere and surface through modules:
- The soil-vegetation module used over tundra and allowing calculation of heat and humidity exchanges between atmosphere and snow- and/or ice-free surfaces [Ridder and Schayes, 1997].
- The snow [Gallée et al., 2001] and ice [Lefebre et al., 2003] module used over snow-covered tundra, sea ice and ice sheets.

The SISVAT snow/ice model is an energy balance model that calculates the exchanges between sea ice, snow-covered tundra or ice sheets on the one hand and atmosphere on the other. It contains multiple modules, namely, thermodynamic, water balance, turbulence, snow blowing, surface albedo, snow/ice discretization and snow metamorphism modules (Figure 2.3) [Fettweis, 2006]. As mentioned, these modules were inspired by the CROCUS snow model developed at the CEN. Gallée et al. [2001]; Lefebre et al. [2003]; Gallée and Duynkerke [1997] have described the physical processes and the validation of MAR.

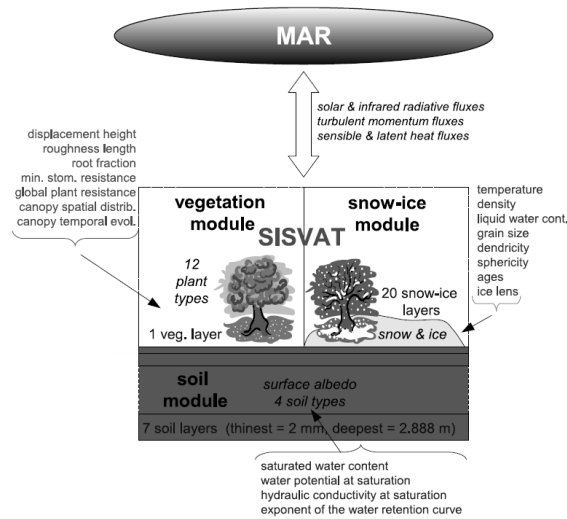FIGURE 2.3: General description of SISVAT. Source: [Fettweis, 2006]

The soil/snow energy balance is solved by the thermodynamic module, whereas the water balance module computes the mass conservation equation for a snow layer in the presence of meltwater run-off, melting snow, refreezing, deposition and accumulation. On low slopes, the accumulation of meltwater can be observed at the surface. Moreover, the parametrization of snow metamorphism comes from the CROCUS model and characterizes snow state on the basis of temperature gradient, density, age of the snow layer and size and the shape of snow grains (called dendricity). This makes it possible for the snow/ice discretization module to divide the snow pack into several layers of variable thickness. The total amount of snow layers may change during a simulation, but the maximum is fixed at 30 layers. Finally, the surface albedo module calculates the snow albedo based on the shape and size of the grains, the thickness of the snow pack, the amount of meltwater, the presence of ice, cloudiness and the solar zenith angle. Practically, the albedo decreases until it reaches the minimum value of 0.65, while snow transforms into firn. The albedo of firn ranges from the minimum value of snow albedo and the maximum value of ice albedo (0.55). Furthermore, its value is deduced using a density equation. The albedo of ice decreases from 0.55 to the minimum value of 0.35 when meltwater appears at the surface. Nevertheless, if the snow pack is thinner than 10 cm, the total albedo will be a combination of that of ice and snow. In addition, the albedo computation takes into account the near-infrared wavelengths absorbed by clouds, resulting in snow absorbing at a similar wavelength range [Fettweis, 2006; Kittel et al., 2016; Lefebre et al., 2003; Tedesco et al., 2016].

Finally, the progressive evolution of the albedo, its correlation with water accumulation and the processes whereby meltwater refreezes make the MAR model unique [Reijmer et al., 2012].

2.2.4 Configuration and simulation set-up

Before launching MAR, initial conditions must be defined using a preprocessing tool called the Nesting Organization for the Preparation of Meteorological and Surface Fields

in Regional Climate Models (NESTOR). During the preprocessing, the integration domain and grid size are determined. NESTOR invokes the time and spatial varying large-scale forcing fields and the data of surface features including soil type, topography, vegetation, etc.

The most recent version of MAR (3.9) was used over the period from 2000 to 2015. It is important to stabilize the model before it can provide consistent data. To do this, it has to simulate climate during a certain amount of time referred to as "spin up". This is the necessary running time before the model outputs become independent of the prescribed initial conditions. The results yielded during this period are unusable [Scholzen, 2015]. In this study, the spin-up time was 16 months (1 year and 4 months), as simulations started in September. Starting after the melt period prevented errors expected from the initial state of snow cover and its thickness. For example, if the simulation had been launched during summer with the wrong amount of snow, due to a rapid melt of the overlying snow, the state of free ice could have appeared earlier. The earlier exposure of permanent ice at the surface would have led to over accelerated melting.

Simulation	SIT	Forcing at ocean surface	*mzhyd*	*mzabso*
GRz0	0.5	ERA-interim	8	5
GRz1	0.1	ERA-interim	8	5
GRz2	1	ERA-interim	8	5
GRz3	2	ERA-interim	8	5
GRz4	5	ERA-interim	8	5
GRz5	10	ERA-interim	8	5
GRm0	0.5	OSTIA	8	5
GRm1	0.1	OSTIA	8	5
GRm2	1	OSTIA	8	5
GRm3	2	OSTIA	8	5
GRm4	5	OSTIA	8	5
GRm5	10	OSTIA	8	5
GRn0	0.5	GLORYSv2.4	8	5
GRn1	0.1	GLORYSv2.4	8	5
GRn2	1	GLORYSv2.4	8	5
GRn3	2	GLORYSv2.4	8	5
GRn4	5	GLORYSv2.4	8	5
GRn5	10	GLORYSv2.4	8	5
GRw0	0.5	ERA-interim	4	3
GRw1	0.1	ERA-interim	4	3
GRw2	1	ERA-interim	4	3
GRw3	2	ERA-interim	4	3
GRw4	5	ERA-interim	4	3
GRw5	10	ERA-interim	4	3
GRt0	Time & spatial varying	GLORYSv2.4	8	5

TABLE 2.3: Ensemble of simulations. (Sea Ice Thickness [SIT] is in meters)

Altogether, 25 simulations were compared in this study (Table 2.3). The first line of the table (*GRz0*) is considered the reference simulation. Similarly, the last line (*GRt0*) is also crucial, as it shows the simulation taking into account time and spatial varying values for SIT. In other words, each grid point sees its SIT imposed at every time step. In contrast, each of the other 24 simulations is characterized by a fixed SIT, ranging between 0.1 m and 10 m. These 24 runs can be divided into four classes. The first three (*GRz*, *GRm* and *GRn*) are based on different reanalyses to constrain the ocean's surface. The

last runs (*GRw*) differ from *GRz*, *GRm* and *GRn* in the configuration of the upper-air relaxation (*mzabso*) and maximum cloud top (*mzhyd*). For more information about *mzabso* and *mzhyd*, see Section 2.2.4 below.

Lateral boundary conditions and upper-air relaxation

MAR is forced at its lateral boundaries every 6 hours depending on a dynamic relaxation procedure [Marbaix et al., 2003]. The lateral boundary conditions (LBCs) comprise surface pressure (SP), temperature (T), two wind components (U and V) and specific humidity (Q) at each vertical level, as well as SST and SIC above the ocean. Note that for the *GRw* simulations (Table 2.3), SIT was added to the LBCs of the ocean's surface. Finally, it is crucial to be aware that temperature is fixed at -2 °C below the sea ice. Thus, if sea ice is present, the temperature at its top is computed on the basis of the thermal diffusion and energy balance equation. Then, depending on the fraction of ice and ocean, skin temperature is proportionally calculated using SST and the temperature on top of the sea ice. Note that in our study, a distinction was made between the near-surface temperature, which is computed at 2 m, 4 m and 8 m above the surface, and the skin temperature, which is the temperature precisely at the surface.

In addition to nudging at its lateral boundaries, MAR includes upper-air relaxation (UAR). This reduces the freedom and hence prevents the model from evolving freely in the highest atmospheric layers. For MAR, the relaxation is applied on the temperature (T) and wind components (U and V) only in the upper part of the atmosphere, by using indiscriminate nudging. There is also a second and potentially better way to proceed based on spectral nudging, although this is computationally more expensive [van de Berg and Medley, 2016]. Indiscriminate nudging is defensible, as only the upper atmosphere is smoothly blended towards the large-scale forcing fields. Thereby, UAR enables retention of the resolved inter-annual variability of ERA-interim whilst maintaining the enhanced spatial patterns determined by the RCM. In contrast, without the UAR, the free evolution of the model would partly remove the real inter-annual variability and therefore reduce the correlation with *in situ* observations [van de Berg and Medley, 2016].

According to Pohl and Crétat [2014]; Omrani et al. [2012], both spectral and indiscriminate nudging improved the representation of precipitation fields and surface climate. These studies show that wind and temperature are the most crucial fields to constrain by nudging.

MAR is divided into 24 layers, decreasing with altitude. The number of layers influenced by the UAR are defined by the parameter *mzabso* during the configuration of MAR. In this manner, *mzabso* fixed at 8 induces a forcing increasing from 0% at layer 7 to 100% at layer 1 (Figure 2.4). Another crucial parameter is *mzhyd*, namely, the level above which micro-physical processes are no longer involved, resulting in the absence of clouds. Similarly, if *mzhyd* is defined as 5, then no clouds will be observed from layer 4 to the top of the atmosphere (see Figure 2.4). The model must be constrained as much as possible, and in the meantime, it must be capable of creating its own clouds. There is an equilibrium to reach between these two parameters, but the maximum height for clouds has to be realistic.

In every simulation in Table 2.3, the ERA-interim reanalysis is employed as forcing fields for Q, U, V, T, SP, both at the lateral boundaries and in the upper-air relaxation zone.

Layers	Altitude (m)	Altitude (10^{-3} hPa)
1	16299	0,0902
2	14080	0,1272
3	12183	0,1706
4	10533	0,2202
5	9081	0,2761
6	7766	0,3387
7	6516	0,4089
8	5311	0,4869
9	4168	0,5719
10	3124	0,6605
11	2221	0,7464
12	1494	0,8221
13	957	0,8825
14	589	0,9263
15	352	0,9555
16	205	0,9739
17	117	0,9850
18	67	0,9915
19	37	0,9952
20	21	0,9973
21	12	0,9984
22	8	0,9990
23	4	0,9995
24	2	0,9997

100% forcing

50% forcing

0% forcing

mzhyd = 5 for *GRz, GRm, GRn* and *GRt.*
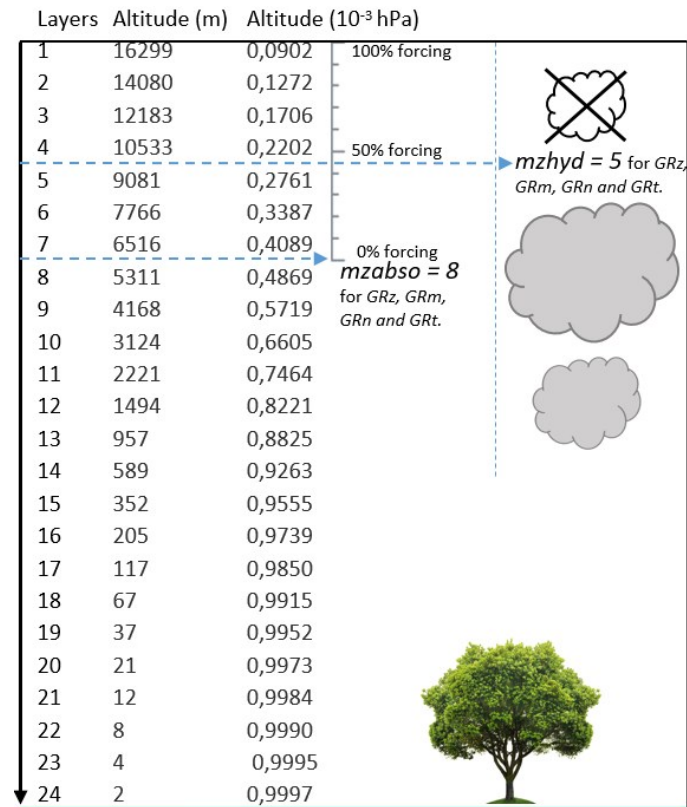
mzabso = 8 for *GRz, GRm, GRn* and *GRt.*

FIGURE 2.4: Representation of the vertical layers of MAR and the upper-air relaxation. In this example, *mzabso* and *mzhyd* are fixed respectively at 8 and 5 as in simulations *GRz*, *GRm*, *GRn*, *GRt*. For *GRw*, *mzabso* is fixed at 4 and *mzhyd* at 3.

However, *GRz*, *GRm* and *GRn* differ by source (ERA-interim, GLORYS2v4 and OSTIA) of SST and SIC.

Domain size and resolution

All the simulations in this study were performed on the Arctic-CORDEX domain (Figure 2.5). The domain is centred on the Arctic Ocean and includes a large portion of land on the edges. The grid size is equal to ± 50 km.

The CORDEX Science Advisory Team (SAT) defined a few requirements for domains to receive the CORDEX designation [WCRP, 2015]:

-Scientific relevance:
Each domain is characterized by specific physical processes, often meso-scale or even smaller. The representation of their space and time-scale can be ensured by providing downscaling techniques. For the resolution of these processes, there must be an added value of RCMs compared with coarser resolution models like GCMs.

-User needs:
A list of the potential users for the downscaled climate information must be established. In addition, the community that will benefit from the downscaling of the region's climate has to be identified.
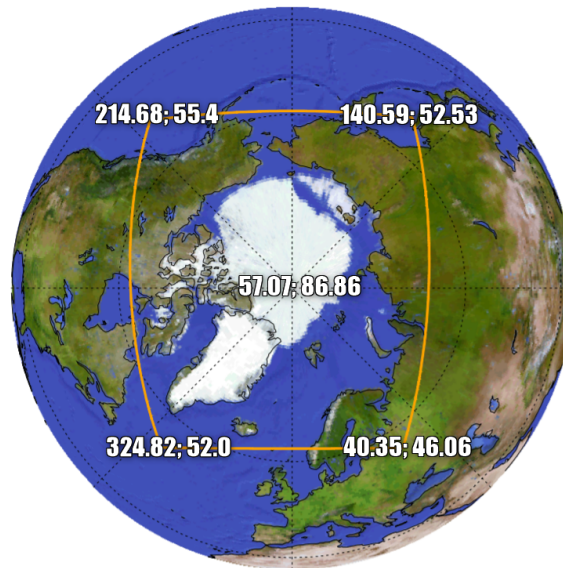
FIGURE 2.5: CORDEX-Arctic domain with coordinates (decimal degrees)
of the corners and the centre. Source: [WCRP CORDEX, 2018]

-Capability requirements:
An assessment of the required computational resources is needed: indeed, there have to
be enough resources to run a large number of simulations on the domain. Moreover, at
least three institutions and three different RCMs must be engaged by the domain. Nat-
urally, the institutions or groups involved must have the necessary resources needed to
perform the downscaling.

-Sensitivity studies performed:
The studies of sensitivity aim to determine the most relevant configuration of the domain.
Often, many simulation runs are needed for this purpose. These studies assess capability
of accurately representing large-scale features such as storm tracks or teleconnections.

These criteria are highly recommended when defining a domain, even outside the
CORDEX program. The domain must be large enough to develop its own internal cir-
culation dynamics [Giorgi, 2011]. For instance if the domain is too small, precipitation is
often underestimated, resulting essentially from the online cloud scheme and less from
the large-scale forcing [Lang, 2011]. On the other hand, in order to maintain a reasonable
computing time and storage, the domain and grid size cannot exceed a critical size. Fi-
nally, high topographical features near the domain's lateral boundaries must be avoided,
because they could lead to inconsistencies between the flow fields of RCMs and GCMs
[Marbaix et al., 2003]. This happens when the coordinate system is hydrostatic and where
the vertical layers depend on the topography.

In conclusion, some elements favour a higher resolution and larger domain, while
others work against them. It is up to the modeler to reach that compromise and find the
most suitable configuration for the model. There is no rule except that the influence of
the configuration of the model on its simulations must be minimized [Giorgi, 2011].

-Configuration of the model:
The parameters (resolution, coordinates of the boundaries, number of grid points...)
of the interior domain (area left once the relaxation zone is removed) must be provided.

The lateral boundary enclosed by a nested RCM and its surrounding large-scale GCM is called the "relaxation zone" or "nudging zone". An abrupt change of wind pattern and grid size between the models will cause distortions of mass and energy fluxes in the nudging zone. For this reason and in order to smoothen the blending between the large-scale boundary conditions and the highly resolved RCM, relaxation functions are involved [Zhong et al., 2010; Scholzen, 2015]. The width of this intermediate area is variable and depends, *inter alia*, on the size of the domain. In our study, and for MAR in general, the relaxation zone amounts to seven pixels. However, inconsistencies often persist, leading to the removal of some additional grid points (four in this study) referred to as the "buffer zone".

Model Calibration

The last step in climate model configuration is tuning, or calibration. Calibration is essential to assess the agreement between the model and available measurements. In our study, a three-year period, from 2009 to 2011, has been selected for the tuning. Obviously, if applied to another period than the one used for calibration, the results are unlikely to be as close to the observations [Scholzen, 2015]. In addition, one has to be aware that well calibrated model processes could compensate for model errors that may not originate from the parametrization. Calibration can be used to hide model deficiencies [Murphy et al., 2007]. Therefore, transparent calibration is preferable to determine whether results arise from the tuning or the model's structure [Bellprat et al., 2012]. As explained in Section 2.2.4, the main parameters we played on to calibrate MAR were *mzabso* and *mzhyd*.

2.2.5 Added value and model development

To conduct this study, it was not sufficient to simply run the model. Three different tasks were identified: interpolation of the ocean reanalyses, modifications of NESTOR routines and changes in the MAR code. This section provides more detail on these specific tasks.

Interpolation of input data

The configuration of the MAR model is such that the use of ERA-interim reanalysis as forcing fields for the lateral boundary conditions is automatic. However, here we aimed to replace the forcing fields of SST and SIC from ERA-interim with those of other reanalyses (GLORYS2v4 and OSTIA). To this end, the first step was to interpolate the high resolution large-scale reanalyses on the broadly resolved Arctic domain of MAR.

In total, two interpolation subroutines were created for both reanalysis and a third one for simulations requiring time and spatial varying SIT. Each of them had a similar core, namely, averaging the pixels of the high-resolution grid on the corresponding MAR pixel.

More specifically, we created a loop browsing MAR's grid points one by one, and for each of MAR's sea pixels, we carried out the following measures:

i) Identification of the coordinates of the corners.

ii) Calculation of the distance from the centre to the four edges of the pixel.

iii) Creation of a box based on the greatest of these four distances.

iv) Identification of the grid points on the high-resolution grid, included in the box created at (iii).

v) Increase of the size of the box created at (iii) if no pixels were identified at (iv).

vi) Averaging of the SST, SIC and/or SIT of the pixels identified at (iv).

Note that the interpolation of a plane grid onto a sphere induces errors that are not taken into account in most RCMs, including MAR.

Modifications in NESTOR

As explained earlier, NESTOR is the MAR's preprocessing tool, and for this purpose, it calls up the large-scale time and spatial varying forcing fields (including SST, SIT, SIC). When SIT is a fixed parameter, the modification of NESTOR's code is limited to the call of a subroutine interpolating the SST and SIC. In contrast, if a simulation must take time and spatial varying SIT into account, changes are made in several other files as well. In this study, the job was simplified by the high commonality between the adjustments needed for SIT and the existing developments concerning SIC.

Modifications in MAR

As for NESTOR, some modules of the MAR model were modified in order to take the additional SIT parameter into account. However, no adjustments were needed in MAR's code for the replacement of the forcing sources of the SIC and SST. In some files, the adaptations made followed the same methodology as used for NESTOR, namely, adjusting the existing developments of SIC for SIT. For other files, the developments were more complex. They consisted of calculating the total depth of sea ice by summing the snow layers with a density superior to $900\ kg/m^3$. The layers of snow had to be removed, as SIT from the reanalyses was composed of ice only. Then, each ice layer calculated by MAR was adjusted in proportion to its thickness, in order to get a total SIT equivalent to the one from GLORYS.

Chapter 3

Hypothesis

i)

Forcing MAR at each time step by SIT reanalyses instead of fixing 0.5 m thickness will reduce surface temperature bias. We will therefore get a better representation of MAR's boundary layer over the Arctic. If this is the case, coupling MAR with NEMO will be considered.

ii)

If SIT is a fixed parameter in the model set-up, the thicker its set, the lower the surface temperature will be in our simulations. For example, if we fix a permanent thickness of 10 m instead of 0.5 m, following the insulation effect of sea ice (Chapter 1), less heat will travel upward through sea ice from the ocean to the overlying air. So we expect the temperature above sea ice to be colder.

iii)

Driving MAR with higher resolution SIC and SST reanalyses (OSTIA, GLORYS) instead of ERA-interim, will yield more accurate outputs (i.e. closer to *in situ* observations).

Chapter 4

Results

This chapter is divided into four sections. First, the reliability of the employed *in situ* time-series is discussed and the evaluation of our simulations is provided. Next, charts explain the influence of SIT on MAR simulations. Similarly, the third section relates to the influence of SIC and SST reanalyses on the MAR's boundary layer. Finally, we discuss the impact of SIT when MAR evolves more freely.

4.1 Evaluation

To assess the accuracy of MAR simulations, the model outputs were compared to observations (reference data) over a specific period in the past. A similar approach was used previously to carry out the calibration (Chapter 2). However, the evaluation did not aim to calibrate the parameters of MAR, such as in Chapter 2, but rather to estimate its performance and capability to represent climate.

Care must be taken that the reference data was obtained from meteorological stations, in other words, at isolated locations, whereas the simulated results are gridded implying a smoothing of extremes [Kotlarski et al., 2014]. In our simulations, the value of each pixel represents an average over a 50 x 50 km^2 surface. As a result, the coarse resolution of our simulations can partly explain the differences between both datasets.

For this reason, modelers often compare their results with gridded reference datasets, such as those from the Climatic Research Unit (CRU) or gridded data coming from the interpolation of meteorological measurements. Unfortunately, *in situ* observations are sparse over the Arctic domain selected for our study; thus their interpolation would inevitably lead to a smoothing of spatial variability [Scholzen, 2015]. Alternatively, re-analyses or remote sensing products can be used for the evaluation. However, as they are derived from models, they carry uncertainty. In addition comparing reanalysis with outputs from a model forced by the same reanalysis is meaningless for determining the performance of the model.

Here, data from 15 single stations has been used to evaluate MAR simulations. For this purpose, each station is linked to the nearest pixel on the domain. The choice of the pixel is based on the minimization of distance between the isolated stations and the centre of the grid-cells.

We assume here that a period of three years (2009-2011) was long enough to get an accurate estimation of the quality of the simulations. Correlation, root mean square error (RMSE), centred root mean square error (RMSEC), bias and standard deviation (STD) were the statistics used to evaluate MAR simulations. The location of the stations was crucial to spatially assess the accuracy of the outputs of the model (see Figure 2.1).

4.1.1 Station selection and evaluation of *GRz0*

Prior to the evaluation of our simulations, we selected the most relevant stations among the whole set. For this purpose, each station was compared independently to the reference simulation *GRz0*. The statistics resulting from the comparison identified the stations that would be preferable to omit due to errors in the time-series. Some time-series contained too many missing values, and furthermore we could not ensure that all the errors were detected by the quality controls. In addition, we could not ignore the possibility of observational instruments inserting artefacts of non-climatic origin into the time-series.

The aim here was not to estimate the accuracy of *GRz0*. We are aware that *GRz0* does not represent the exact state of the atmosphere. Thus, the stations were not omitted because of inconsistencies with *GRz0* but rather by comparing the statistics obtained for each station.

The remaining stations were then averaged to obtain three observational datasets (for precipitation, near-surface temperature (at 2 m) and sea level pressure), used as references for comparing the simulations. At that point, the aim was to assess the accuracy of each simulation, namely, the evaluation of MAR simulations.

Before proceeding, the number of "credible" values of precipitation, near-surface temperature and sea level pressure are presented in Table 4.1. By "credible" we mean the ones that were realistic and successfully went through the prerequisite checks we imposed. Table 4.1 shows that we did not include the following stations in the statistics for precipitation: Angisoq (ECA&D), Daneborg (ECA&D), Angisoq (NOAA), Daneborg (NOAA), Kotlas and Taloyoak. In contrast, the number of "credible values" did not conduct us to omit stations for temperature or SLP statistics.

		Number of daily measurements over 2009-2011		
Database	Station	Temperature (2m)	Precipitation	Sea level pressure
ECA&D	Angisoq	706	0	1084
	Daneborg	562	0	873
	Hopen Island	1092	1095	1094
	Reykjavik	1092	1095	1095
	Tasiilaq	792	1060	1041
NOAA	Angisoq	1061	0	1061
	Angoon	883	632	714
	Daneborg	869	0	869
	Hopen Island	1095	1082	1093
	Kivalina Airport	1088	1073	1085
	Kotlas	1084	2	1084
	Ougolny Airport	1064	361	1062
	Taloyoak	1079	0	1079
	Thule Air Base	1092	524	1089
	Tiksi	1095	786	1077

TABLE 4.1: Number of daily measurements per station for near-surface temperature, precipitation and sea level pressure over a total of 1,095 days (3 years). Stations in blue are stations for which time-series were taken from NOAA and ECA&D. Red values are values inducing the removal of the station for the evaluation of MAR simulations

First, for near-surface temperature (2 m), as most of the stations had a correlation exceeding 0.9, we could assume that the others contained errors. Therefore, three stations were omitted: Angisoq (ECA&D and NOAA) and Angoon (NOAA) (Table 4.2). We also considered that stations showing an absolute value of bias superior to 3°C would be removed, which also led us to eliminate Hopen Island (ECA&D and NOAA). On basis of the large heigh difference between the weather stations and the corresponding MAR pixels, it was not surprising for these stations to show great near-surface temperature biases and weak correlations (Table 2.2). The great difference in altitude (>100 m) was a major reason for the removal of these five stations. Despite this, the remaining stations displayed a very high correlation with *GRz0*, often above 0.95. Finally, the RMSE of each station was lower than the respective standard deviation in Table 4.2, meaning that the RMSE was not significant following the convention in climatology [Delhasse et al., 2017]. As a result, none of the stations was omitted for this criterion.

Database	Station	Temperature (2 m) (°c)				
		Correlation	Mean Bias	CRMSE	RMSE	STD
ECA&D	Angisoq	0.86	-0.80	2.85	2.96	3.53
	Daneborg	0.95	1.94	3.24	3.78	9.99
	Hopen Island	0.93	-3.55	3.88	5.26	6.81
	Reykjavik	0.96	-0.56	1.44	1.54	5.27
	Tasiilaq	0.93	-1.44	2.62	2.99	6.20
NOAA	Angisoq	0.70	-3.85	4.17	5.68	4.59
	Angoon	0.60	-4.53	7.75	8.97	9.63
	Daneborg	0.95	2.08	3.28	3.89	10.08
	Hopen Island	0.93	-3.57	3.88	5.27	6.80
	Kivalina Airport	0.96	-0.64	3.83	3.88	12.74
	Kotlas	0.97	-1.99	5.49	5.84	13.06
	Ougolny Airport	0.97	-1.12	3.38	3.56	14.15
	Taloyoak	0.97	0.04	4.43	4.43	15.54
	Thule Air Base	0.96	2.16	3.59	4.19	12.12
	Tiksi	0.97	0.03	4.79	4.79	15.65

TABLE 4.2: Near-surface temperature statistics (bias, correlation, RMSE, CRMSE and STD) for all the stations. Blue stations are stations mentioned twice. Red values are values inducing the removal of the station for the evaluation of MAR simulations

Regarding precipitation, a large selection had already been made on the basis of the amount of "credible" values of each dataset. Here, most of the remaining stations must be set aside due to significant RMSE values. The RMSE is more than twice as high as the standard deviation for all the NOAA stations (Table 4.3). Moreover, the correlations for precipitation are considerably lower than they are for temperature. This is not surprising since precipitation includes snowfall, which is difficult to measure and precipitation is more complicated to simulate than temperature. Thereby, the station of Tasiilaq has the highest correlation (0.54) and by contrast, Thule Air Base has the lowest (0.08).

Finally, for sea level pressure, 10 stations out of 15 were selected. Two of the five rejected stations (Angoon and Tiksi) presented a considerable standard deviation (STD) (Table 4.4). The STD reached 397.9 for Angoon and 129.64 for Tiksi (Table 4.4). And as the STD reflects the daily variability of the observations, we expected that errors may have occurred during the measurement or treatment of the data. The great biases computed

		Precipitation (mm)				
Database	Station	Correlation	Mean Bias	CRMSE	RMSE	STD
	Hopen Island	0.33	0.17	1.92	1.93	1.70
ECA&D	Reykjavik	0.36	-0.56	3.61	3.65	3.65
	Tasiilaq	0.54	-1.26	5.65	5.97	6.83
	Angoon	0.34	2.94	4.50	4.55	0.31
	Hopen Island	0.26	0.92	1.58	1.82	0.16
	Kivalina Airport	0.29	0.56	1.51	1.60	0.17
NOAA	Ougolny Airport	0.49	0.96	1.79	1.18	0.31
	Thule Air Base	0.08	1.08	2.82	2.09	0.68
	Tiksi	0.35	0.18	0.77	0.67	0.27

TABLE 4.3: Precipitation statistics (bias, correlation, RMSE, CRMSE and STD) for stations having more than two observations. Blue stations are stations mentioned twice. Red values are values inducing the removal of the station for the evaluation of MAR simulations.

for the three other stations (Tasiilaq, Angisoq (NOAA) and Thule Air Base) were mainly due to the altitude difference between MAR pixels and the stations (Table 2.2). This can be demonstrated by the difference between the RMSE and the CRMSE. Before moving to the evaluation of MAR simulations, note that the correlations for the SLP were significant (>0.9) and even better than for the near-surface temperature (see Table 4.2).

		Sea level pressure (hPa)				
Database	Station	Correlation	Mean Bias	CRMSE	RMSE	STD
	Angisoq	0.97	-20.89	3.00	21	12.24
	Daneborg	0.96	-19.20	3.22	19.59	10.55
ECA&D	Hopen Island	0.97	-20.58	3.03	20.80	11 80
	Reykjavik	0.99	-4.96	2.40	5.51	14.14
	Tasiilaq	0.97	-43.48	3.39	43.66	14.15
	Angisoq	0.97	-62.63	3.07	62.70	12.36
	Angoon	0.98	-20.82	2.19	18.82	397.90
	Daneborg	0.97	-19.00	2.83	19.21	11.40
	Hopen Island	0.97	-20.60	2.96	20.80	44.68
	Kivalina Airport	0.96	-11.48	3.31	11.94	54.07
NOAA	Kotlas	0.98	-16.71	2.21	16.86	11.10
	Ougolny Airport	0.95	-17.58	3.24	17.86	45.09
	Taloyoak	0.94	-9.58	3.28	10.13	9.86
	Thule Air Base	0.96	-32.64	3.14	32.74	54.06
	Tiksi	0.97	-14.09	2.92	14.27	129.64

TABLE 4.4: Sea level pressure statistics (bias, correlation, RMSE, CRMSE and STD) for all the stations. Blue stations are stations mentioned twice. Red values are values inducing the removal of the station for the evaluation of MAR simulations

4.1.2 Evaluation of MAR simulations

The statistics resulting from the comparison between *GRz0* and the stations allowed the removal of several datasets (Section 4.1.1). However, stations corresponding to datasets

		Mean Bias		
Reanalysis	**Simulations**	Near-surface temperature	Precipitation	Sea level pre
	GRz0 (0.5m)	0.05	-0.55	-16.06
	GRz1 (0.1m)	0.52	-0.56	-16.26
ERA-interim	GRz2 (1m)	-0.04	-0.55	-16.03
	GRz3 (2m)	-0.14	-0.55	-15.98
	GRz4 (5m)	-0.21	-0.55	-15.97
	GRz5 (10m)	-0.26	-0.54	-15.92
	GRm0 (0.5m)	-0.11	-0.53	-15.92
	GRm1 (0.1m)	0.26	-0.54	-16.07
OSTIA	GRm2 (1m)	-0.22	-0.53	-15.87
	GRm3 (2m)	-0.31	-0.53	-15.83
	GRm4 (5m)	-0.39	-0.53	-15.80
	GRm5 (10m)	-0.41	-0.53	-15.79
	GRn0 (0.5m)	-0.02	-0.55	-16.02
	GRn1 (0.1m)	0.27	-0.55	-16.05
	GRn2 (1m)	-0.24	-0.53	-15.84
GLORYSv2.4	GRn3 (2m)	-0.34	-0.53	-15.80
	GRn4 (5m)	-0.43	-0.53	-15.77
	GRn5 (10m)	-0.44	-0.53	-15.76
	GRt (time and spatial varying)	-0.18	-0.55	-16.18
		Correlation		
All	All simulations	0.96 ± 0.006	0.41 ± 0.006	0.97 ± 0.0
		RMSE		
All	All simulations	3.90 ± 0.1	3.80 ± 0.1	16.30 ± (

TABLE 4.5: Mean daily bias, RMSE and correlation between the simulations (*GRz*, *GRm*, *GRn* and *GRt*) and the averaged near-surface temperature (2 m), precipitation and sea level pressure over the period 2009-2011 of the stations.

with a small probability of error were selected: 10 for temperature, 3 for precipitation and 10 for SLP. In this section, the selected observations have been averaged and compared to the simulations. The resulting statistics are presented in two tables. Table 4.5 includes the simulations with *mzabso* equal to 8 and *mzhyd* to 5, whereas Table 4.6 corresponds to the simulations *GRw* (*mzabso*=4 and *mzhyd*=3).

As for the correlations, they are the same for *GRz*, *GRm*, *GRn* and *GRt* (Table 4.5). Therefore, correlations of 0.96, 0.41 and 0.97 were computed for near-surface temperature, precipitation and SLP, respectively. Similarly, the simulations *GRw0,1,2,3,4* and *5* were equally correlated with the reference data for near-surface temperature (0.91), precipitation (0.31) and SLP (0.84) (Table 4.6). Thus, owing to the reduction of *mzabso* and *mzhyd*, correlations are significantly lower for *GRw* than for the other simulations. As explained in Chapter 2, a reduction of the UAR enables the model to evolve more freely and partly removes the real inter-annual variability.

In the same way, the mean biases are close for each simulation, although differences can be observed for near-surface temperature. Therefore, whatever the reanalyses used as forcing field, the thicker sea ice is fixed, the colder will be the mean daily near-surface temperatures (Tables 4.5 and 4.6). Next to this, we can clearly see that the biases are much

lower for MAR driven by GLORYS2v4 and OSTIA than for MAR driven by ERA-interim (Table 4.5). In addition, the absolute value of the biases of *GRw* (Table 4.6) are much higher for near-surface temperature and lower for SLP than the biases of *GRz, m, n, t* (Table 4.5).

Finally, we can assume that the ensemble of simulations launched in this study are acceptable even if the correlations for precipitation are not convincing. Despite this, the RMSE is not significant for any simulation as it is lower than twice the standard deviation of observations.

		Mean Bias		
Reanalysis	**Simulations**	Near-surface temperature	Precipitation	Sea level pressure
	GRw0 (0.5m)	-0.89	-0.48	-12.93
	GRw1 (0.1m)	-0.37	-0.46	-13.02
ERA-interim	GRw2 (1m)	-1.03	-0.46	-13.09
	GRw3 (2m)	-1.02	-0.47	-12.96
	GRw4 (5m)	-1.14	-0.44	-12.86
	GRw5 (10m)	-1.22	-0.51	-12.89
		Correlation		
All	All simulations	0.91 ± 0.006	0.31 ± 0.006	0.84 ± 0.006
		RMSE		
All	All simulations	5.40 ± 0.1	4.00 ± 0.1	15.00 ± 0.2

TABLE 4.6: Mean daily bias, RMSE and correlation between the simulations (*GRw*) and the averaged near-surface temperature (2 m), precipitation and sea level pressure over the period 2009-2011 of the stations.

4.2   Influence of SIT on MAR simulations driven by ERA-interim

In this section, the effect of SIT on the boundary layer of our simulations will be analysed through the skin temperature only. Figures regarding sea level pressure and precipitation are not displayed here as they remain mostly unchanged by SIT variations.

4.2.1   Skin temperature

Skin temperature ranges from $\pm - 40$ °C above central Greenland, the isles of the Canadian archipelago and the highest plateaus of Russia to ± 10 °C above the North Atlantic Ocean and the North Pacific Ocean. The centre of the North Pole is colder than its surroundings, with a skin temperature equivalent to -30 °C (Figure 4.1a).

Figure 4.1b shows a positive anomaly for *GRz1* (SIT=0.1 m) compared with *GRz0* (SIT=0.5 m), reaching +6°C near the northern coast of North America, western Russia and over Baffin Bay. This figure illustrates the effect of a thinner sea ice pack (0.1 m) on temperature rise above sea ice in winter. Figures 4.1c, 4.1d, 4.1e and 4.1f show the opposite effect, as SIT is fixed at a higher value than for the reference run. The thicker the ice, the stronger the insulation effect of sea ice and the colder the skin temperature observed above the Arctic.

An interesting thing to note is the weak difference between *GRz4* (SIT=5 m) and *GRz5* (SIT=10 m) (Figures 4.1e and 4.1f). Although the difference of SIT between both runs is 5

m, the anomalies are very similar.

Finally, Figures 4.1b, 4.1c, 4.1d, 4.1e, and 4.1f show a great anomaly above the Arctic Ocean, but the skin temperature remain unchanged above the surrounding continents when the SIT is changed. In other words, the effect of SIT is mostly local.
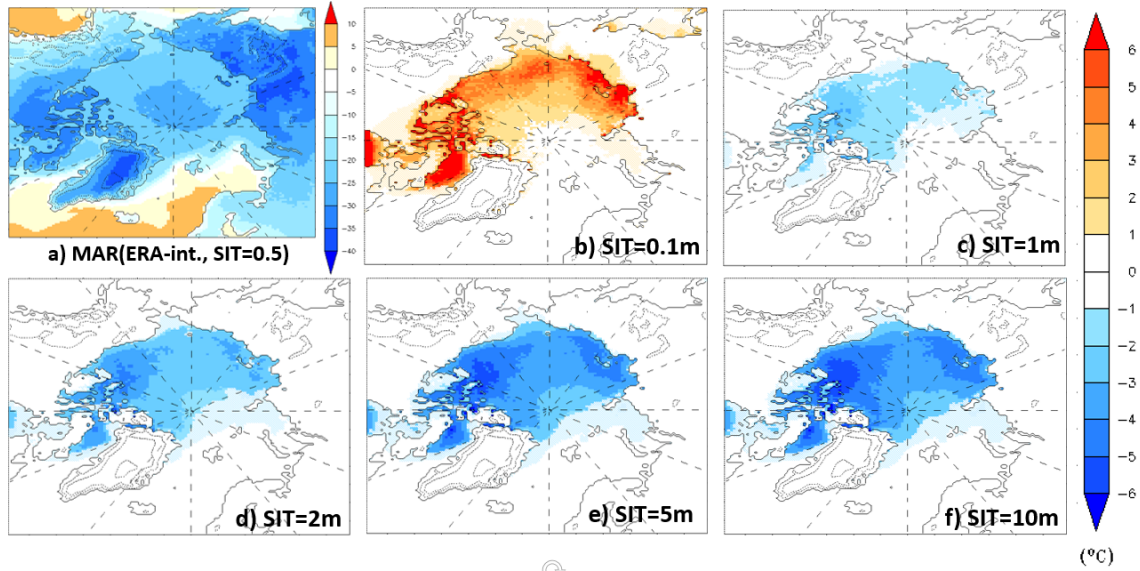

FIGURE 4.1: **a)** Mean skin temperature for DJF modeled by MAR forced by ERA-interim with 0.5 m SIT over 2000-2015. **b to f)** Mean skin temperature anomaly for DJF modeled by MAR over 2000-2015. Or MAR(ERA-int., SIT=?) - MAR(ERA-int., SIT=0.5).
(Hatched = insignificant)

4.3 Influence of the reanalyses on MAR's boundary layer

As the different reanalyses used in this study have a weak influence on sea level pressure, the results displayed in this section focus on skin temperature and precipitation.

4.3.1 Skin temperature

Figure 4.2 is similar to Figure 4.1, but instead of comparing MAR driven by ERA-interim with a varying SIT, it compares MAR forced by different reanalyses with a fixed SIT (0.5 m).

First, the skin temperature anomaly displayed in Figure 4.2b highlights the lack of benefit of using OSTIA instead of ERA-interim reanalysis in MAR. Despite the high resolution of OSTIA, the differences in skin temperature are sparse and insignificant.

Similarly, the benefit of driving MAR with the intermediate reanalysis GLORYS2v4 is insignificant (Figure 4.2c). Note that the areas with the highest anomalies are common for MAR based on GLORYS and on OSTIA, although anomalies are larger and even significant in some spots concerning GLORYS. These areas are located over the Greenland Sea, along the East Asian coast and around the Canadian Archipelago, so mainly at the margins of the ice sheet. Concerning the inlet extending from the Kara Sea, there must be

an interpolation error, as the skin temperature anomaly is strongly positive locally (Figures 4.2c and 4.2d).

For MAR simulations considering time and spatial varying SIT from GLORYS, skin temperatures have nothing to do with MAR outputs forced by GLORYS with a fixed 0.5 m SIT (Figure 4.2d). In contrast, Figure4.2d is very close to Figure 4.1d.
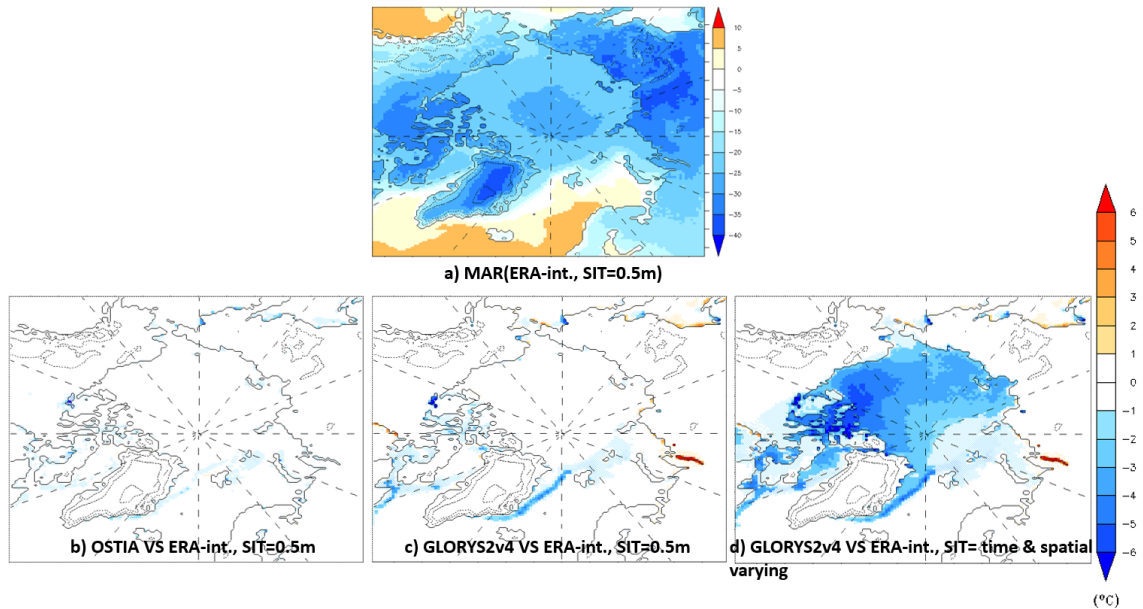

FIGURE 4.2: **a)** Mean skin temperature for DJF modeled by MAR forced by ERA-interim with 0.5 m SIT over 2000-2015. **b to d)** Mean skin temperature anomaly for DJF modeled by MAR over 2000-2015. Or MAR(reanalysis=?., SIT=0.5) - MAR(ERA-int., SIT=0.5).
(Hatched = insignificant)

4.3.2   Precipitation

Figure 4.3 is similar to Figure 4.2, but instead of studying the influence of the reanalyses on MAR's skin temperature, it focuses on its impacts on mean annual precipitation.

Mean annual precipitation (rainfall and snowfall) ranges from ±50 mmWE/yr above central Greenland, the isles of the Canadian archipelago and the Arctic Ocean to ±1500 mmWE/yr on the west coasts of Norway and Canada and the southern coasts of Greenland and Iceland. Globally, precipitation increases from the North Pole toward the boundaries of our domain (Figure 4.3a).

The precipitation anomalies shown in Figures 4.3b, 4.3c and 4.3d are insignificant over the whole Arctic domain, except regarding the abnormality over the inlet extending from the Kara Sea. We assumed that this abnormality was due to interpolation issues between the grids. However, compared to the reference simulation of MAR (Figure 4.3a), the forcing based on OSTIA simulated stronger precipitation (Figure 4.3b), whereas the forcing based on GLORYS simulated weaker precipitation (Figure 4.3c) especially when time and spatial varying SIT was implemented (Figure 4.3d).

When driven by GLORYS, MAR's skin temperature is lower than when driven by ERA-interim (Figure 4.2c). Thus it is not surprising that rainfall is weaker when using GLORYS as boundary conditions (Figure 4.3c). An, explanation could be that there is less evaporation combined with the fact that cold air can contain less water.
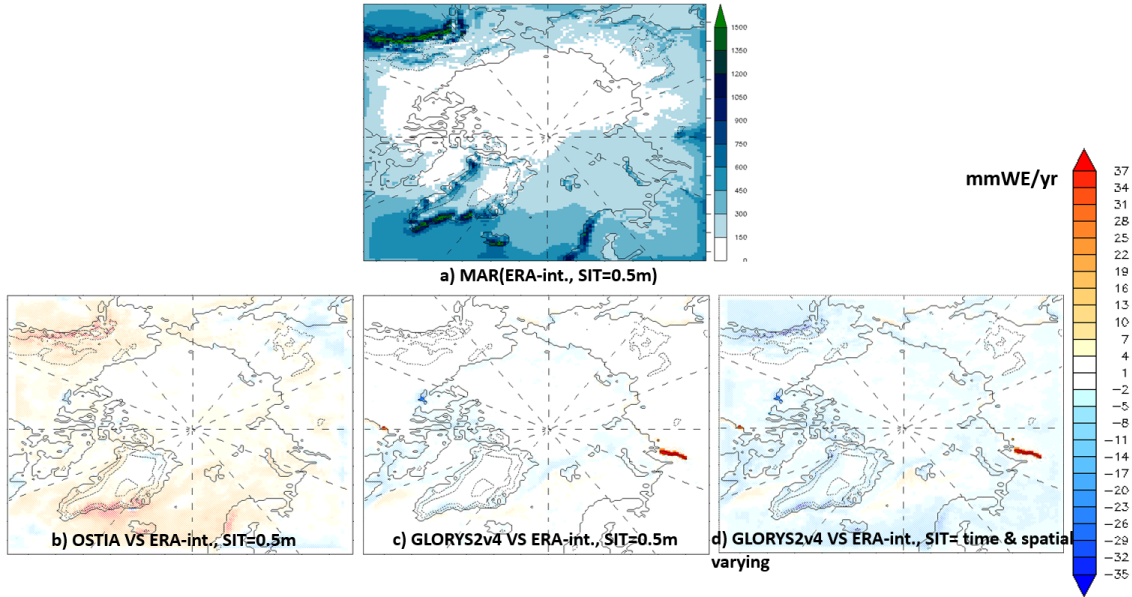

FIGURE 4.3: **a)** Mean annual precipitation modeled by MAR forced by ERA-interim with 0.5 m SIT over 2000-2015. **b to d)** Mean annual precipitation anomaly modeled by MAR over 2000-2015. Or MAR(reanalysis=?., SIT=0.5) - MAR(ERA-int., SIT=0.5).
(Hatched = insignificant)

4.4 Influence of upper-air relaxation

This second section of our results consists of estimating the influence of reduced upper-air forcing (*mzabso*=4, *mzhyd*=3) compared to the original relaxation (*mzabso*=8, *mzhyd*=5). A reduction of the forcing in the upper atmospheric layers allowed the model to evolve more freely. The simulations *GRw* were conducted because we expected a greater influence of SIT on MAR simulations if *mzabso* and *mzhyd* were lowered.

4.4.1 Comparison of *GRz0* and *GRw0*

As seen in Subsection 4.1.2, the anomaly between *GRz* and *GRw* is more pronounced than the anomaly between *GRz* and *GRm* or *GRn*.

As for skin temperatures, they are significantly colder over the isles of the Canadian archipelago, northern Greenland and the North Pole for the less-constrained version of MAR (Figure 4.4b). In addition, reducing *mzabso* and *mzhyd* also significantly impacted mean annual precipitation (Figure 4.5b). The figure shows a positive anomaly reaching more than 100 mmWE/yr over the Greenland Sea and Alaska.
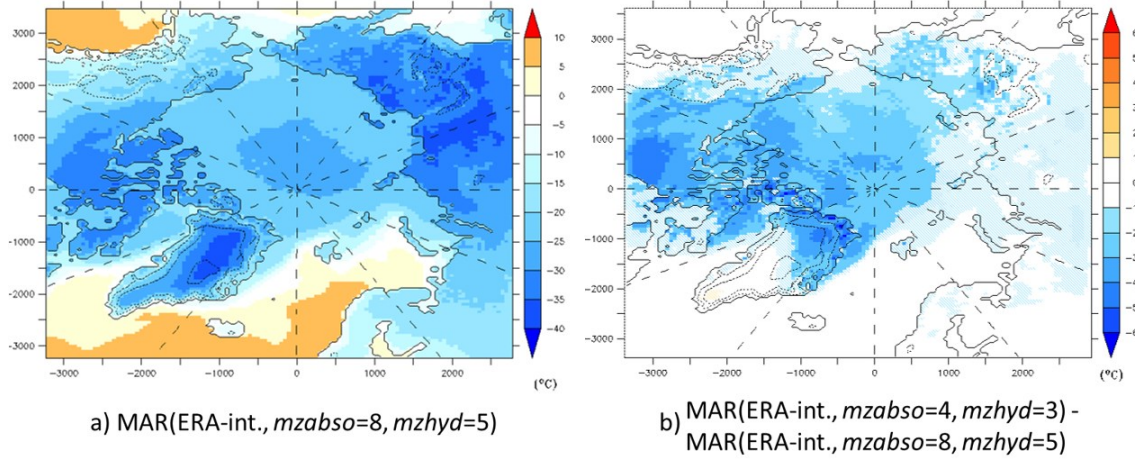
a) MAR(ERA-int., *mzabso*=8, *mzhyd*=5)

b) MAR(ERA-int., *mzabso*=4, *mzhyd*=3) - MAR(ERA-int., *mzabso*=8, *mzhyd*=5)

FIGURE 4.4: **a)** Mean skin temperature for DJF modeled by MAR(*mzabso*=8,*mzhyd*=5,SIT=0.5) forced by ERA-interim over 2000-2015. **b)** Mean skin temperature anomaly for DJF between the constrained and less-constrained set-ups of MAR over 2000-2015. (Hatched = insignificant)
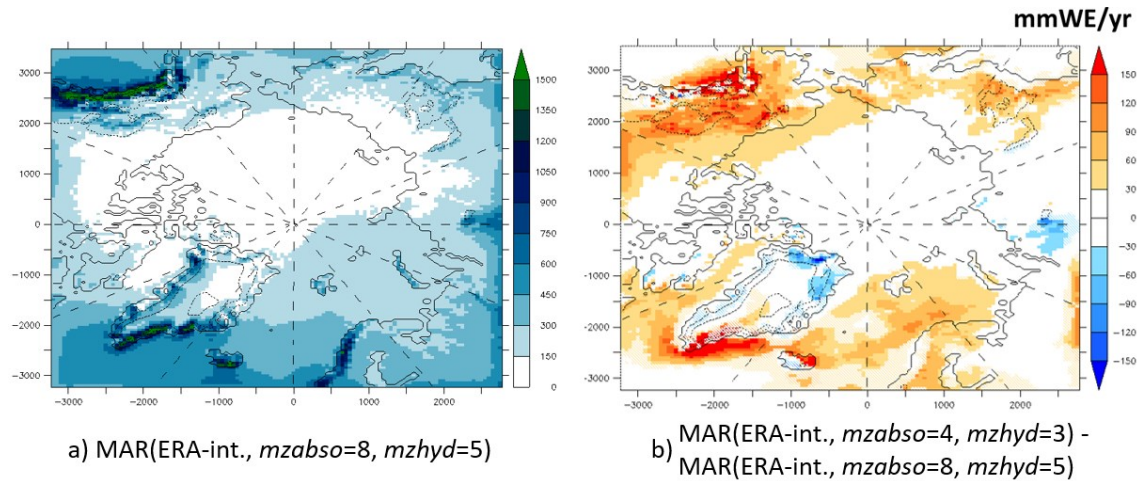

a) MAR(ERA-int., *mzabso*=8, *mzhyd*=5)

b) MAR(ERA-int., *mzabso*=4, *mzhyd*=3) - MAR(ERA-int., *mzabso*=8, *mzhyd*=5)

FIGURE 4.5: **a)** Mean annual precipitation modeled by MAR(*mzabso*=8,*mzhyd*=5,SIT=0.5) forced by ERA-interim over 2000-2015. **b)** Mean annual precipitation anomaly between the constrained and less-constrained set-ups of MAR over 2000-2015. (Hatched = insignificant)

4.4.2 Impact of SIT on atmospheric circulation and skin temperature

Skin temperature

Initially we expected a greater influence of SIT on *GRw* simulations than on *GRz* simulations. However, the anomalies computed within the set of *GRw* simulations were close to the results shown earlier for *GRz* in Figure 4.1. We found the same patterns with a negative skin temperature anomaly, increasing along with the thickening of sea ice. We assumed that the similarity between *GRw* and *GRz* anomalies resulted from the atmospheric circulation changes (Figure 4.9) from year to year for *GRw* simulations. In order to remove that randomness and to get a clear signal, we employed the RMSE instead of the anomaly.

Figures 4.6a and b are similar above the Arctic Ocean and most of the areas covered by water. On the other hand, Figure 4.6b shows a higher RMSE over the continental regions surrounding the Arctic Ocean.
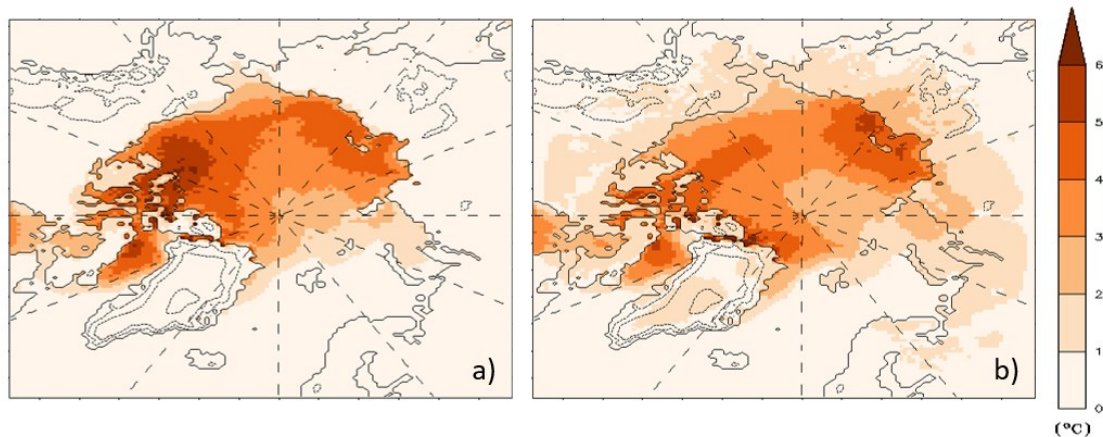

FIGURE 4.6: Root mean square error between MAR(ERA-int,SIT=0.5) and MAR(ERA-int,SIT=10) of mean skin temperature for DJF from 2000 to 2015. **a)** Results modeled by the constrained set-up of MAR (mzabso=8, mzhyd=5). **b)** Results modeled by the less-constrained set-up of MAR (mzabso=4, mzhyd=3).

Wind speed and direction

This section discusses wind speed and direction anomalies at 8 m height and 500 hPa. The reason why we focused on these two heights is that anomalies are stronger at 8m for the near-surface layers (2 m, 4 m, 8 m) and at 500 hPa for the eight higher atmospheric layers provided as output by MAR. There were similar atmospheric circulation patterns at 8 m height for both parametrizations of MAR's upper-air relaxation (Figures 4.7a and 4.7c). In both cases, the strongest winds were situated along the coasts of Greenland (± 10 m/s), over the North Atlantic (± 6 m/s) and locally over most of the coastal regions (± 6 m/s).

Regarding the constrained set-up of MAR (Figure 4.7b), the same wind patterns were computed for MAR based on 10 m SIT and 0.5 m SIT. This is reflected in the figure by the absence of anomaly. On the other hand, if 10 m SIT is prescribed in the less-constrained set-up, then a few spots of positive wind speed (± 0.5 m/s) and negative wind speed (± -0.5 m/s) are observed (Figure 4.7d).

The same analysis was applied at higher altitudes (500 hPa) to assess the effect of SIT on the atmospheric circulation at a larger scale. At 500 hPa, mean wind speeds are much higher than at the surface. They increase from ± 0 m/s at the North Pole to ± 12 m/s over the North Atlantic Ocean and central Canada. The directions of the wind are also different, more homogeneous at 500 hPa than at the surface (Figures 4.8a and 4.8c).

Figure 4.8d highlights the presence of positive (up to 1 m/s) and negative (up to - 1 m/s) anomaly areas over the Arctic. This reflects the significant influence of SIT on upper-atmospheric circulation. In contrast, there is no anomaly when using the most constrained set-up of MAR, i.e. *mzabso*=8 and *mzhyd*=5 (Figure 4.8b). Finally, Figure 4.9 displays the random nature of the impacts of SIT on the wind pattern from one year to
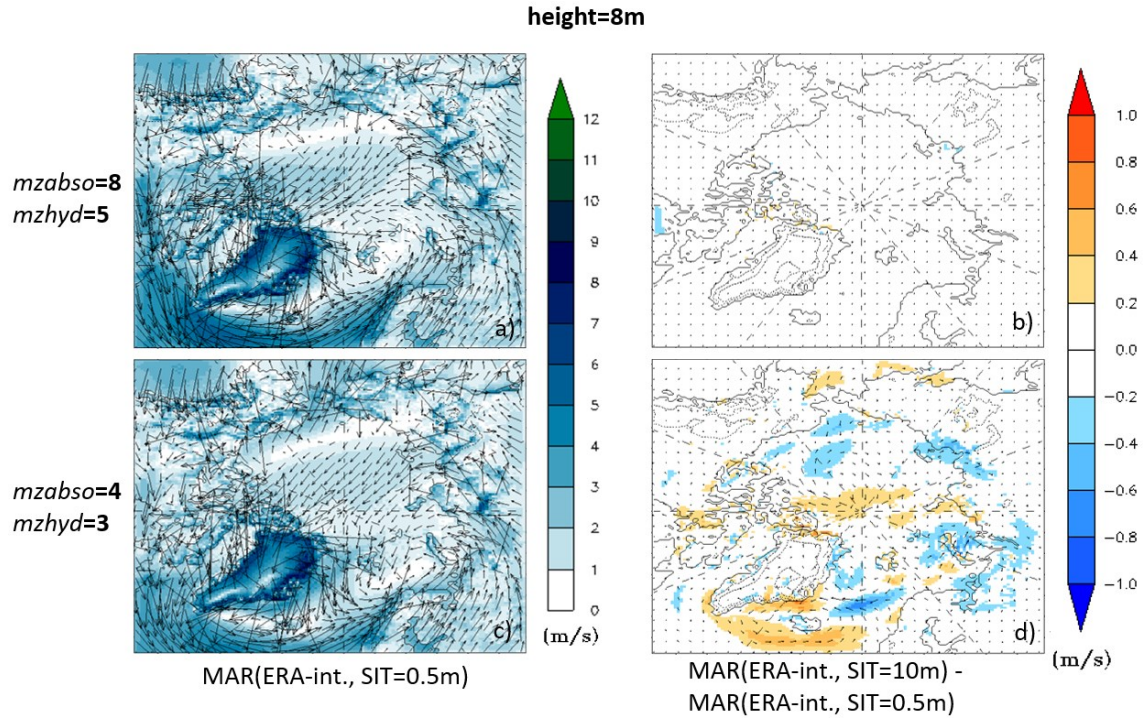
height=8m

FIGURE 4.7: **a and c)** Mean wind speed and direction at 8 m height modeled by MAR forced by ERA-interim with SIT=0.5 m for 2015. **b and d)** Mean wind speed and direction anomaly at 8 m height (10m SIT - 0.5m SIT) for 2015. Or MAR(ERA-int., SIT=10m) - MAR(ERA-int., SIT=0.5m). **a and b)** Results modeled by the constrained set-up of MAR (mzabso=8, mzhyd=5). **c and d)** Results modeled by the less-constrained set-up of MAR (mzabso=4, mzhyd=3).

the next. We can see that the wind speed and direction patterns of the four graphs in figure 4.9 show no similarities.
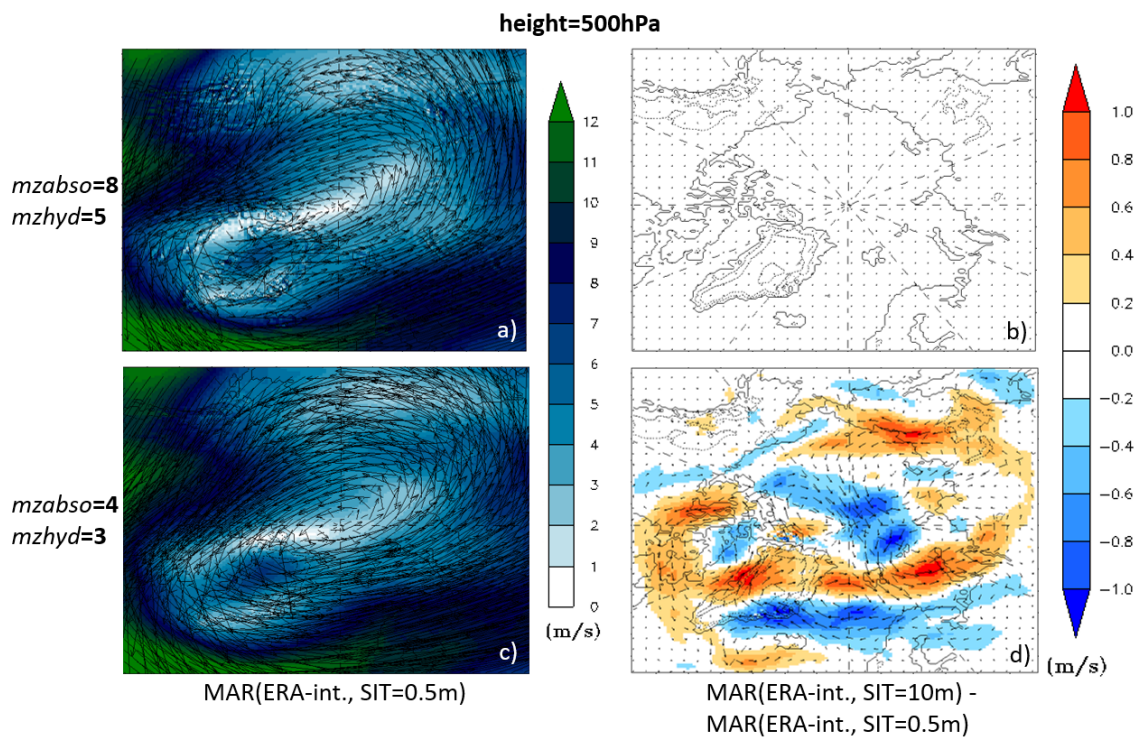
height=500hPa

FIGURE 4.8: **a and c)** Mean wind speed and direction at 500 hPa height modeled by MAR forced by ERA-interim with SIT=0.5m for 2015. **b and d)** Mean wind speed and direction anomaly at 500 hPa height (10m SIT - 0.5m SIT) for 2015. Or MAR(ERA-int., SIT=10m) - MAR(ERA-int., SIT=0.5m). **a and b)** Results modeled by the constrained set-up of MAR (mzabso=8, mzhyd=5). **c and d)** Results modeled by the less-constrained set-up of MAR (mzabso=4, mzhyd=3).
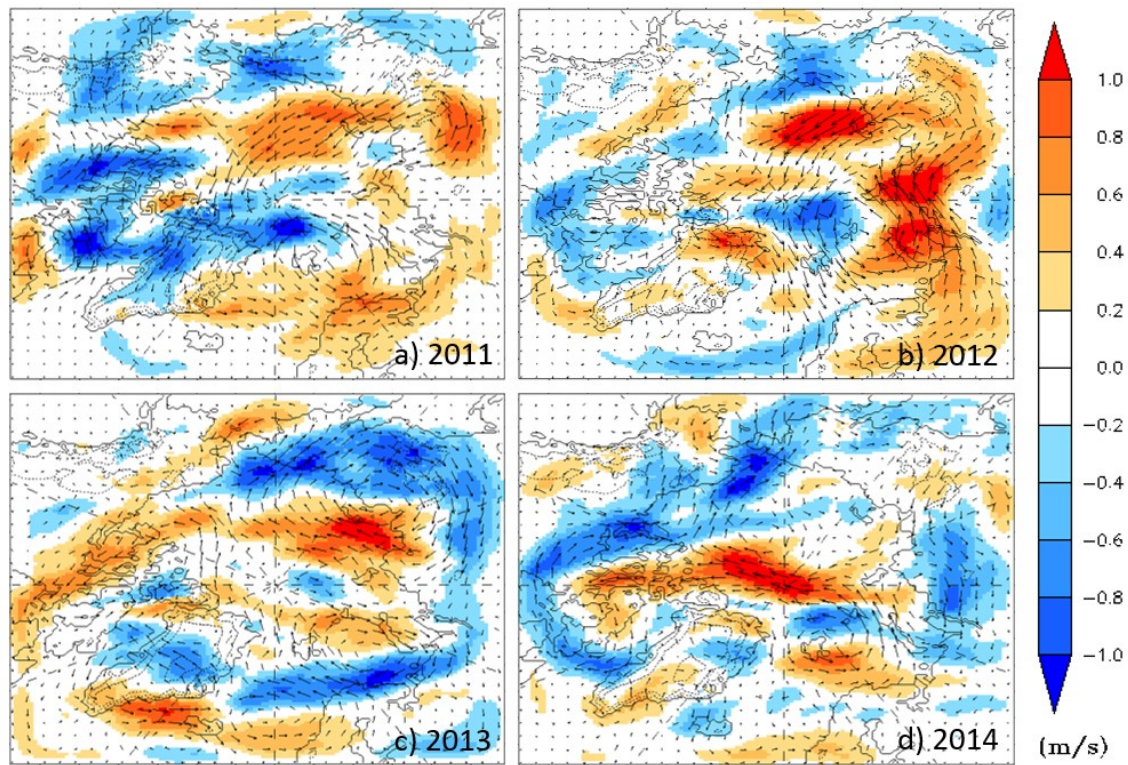
FIGURE 4.9: Mean wind speed and direction anomaly at 500 hPa height (10m SIT - 0.5m SIT) modeled by the less-constrained set-up of MAR driven by ERA-interim for **a)** 2011 **b)** 2012 **c)** 2013 **d)** 2014 . Or MAR(ERA-int., SIT=10m, mzabso=4, mzhyd=3) - MAR(ERA-int., SIT=0.5m, mzabso=4, mzhyd=3).

Chapter 5

Discussion

According to Krinner et al. [2010], the influence of SIT is more pronounced in winter when the temperature gradient between oceanic water and the overlying atmosphere is strong. On the other hand, we expected greater anomalies at the margins of the sea ice pack than at locations with thick sea ice [Rinke et al., 2006]. Yet, we observed insignificant and low anomalies at the margins on the European side of the Arctic Ocean (Figures 4.1b to 4.1f). A plausible reason for this is the influence of surface winds (Figures 4.7a and 4.7c). The spatial variability of wind speed and direction disturbs the distribution of skin temperature. If SIT has a greater influence along the northern Russian coast, the North American coast and the isles of the Canadian archipelago, it may be due to the weaker winds observed in these areas and the blocking effect of continents.

The blocking effect of continents could also explain a second characteristic visible in Figures 4.1b to 4.1f and Figure 4.2d, which is the absence of skin temperature anomaly above continents. We assume that cold air stays in the lower troposphere in winter owing to its higher density. Therefore, the air mass influenced by SIT will not mix with other air masses above the surrounding continents. As a result, the impact of SIT is only local. This is confirmed by Deser et al. [2010], showing that surface air temperature responses are confined under a low-level inversion over Arctic in winter. In addition, Noel et al. [2014] showed that the impacts of SIC and SST do not considerably impact Greenland resulting from the katabatic wind blocking effect.

A second aim was to estimate the impact of SST and SIC reanalyses on MAR simulations. As shown in Figures 4.2b to 4.2c and Figures 4.3b to 4.3c, it turned out that all three reanalyses (ERA-interim, OSTIA and GLORYS2v4) yielded similar results for skin temperature and precipitation. This is not surprising, as they are linked: ERA-interim uses outputs from OSTIA, and GLORYS is based on atmospheric conditions provided by ERA-interim (see Chapter 2). Furthermore, the benefit of using high resolution reanalyses such as GLORYS and OSTIA for the oceanic conditions was small in our study as we interpolated them on the coarse (50 x 50 km) resolution of MAR's grid. At higher resolution (10 km for example) the model would be able to represent polynyas, SST variations and several other small-scale features. In addition, surface pressure anomalies were not included in our work, given that neither SIT nor SIC influenced the simulated pressure fields for the constrained set-up of MAR (*mzabso=8*, *mzhyd=5*).

Concerning the implementation of time and spatial varying SIT into MAR (corresponding to simulation *GRt*), its influence did not extend beyond the Arctic Ocean (Figure 4.3d) and it yielded skin temperatures very much like those from MAR driven by ERA-interim with 2 m or 5 m SIT (Figures 4.1d and 4.1e). In addition, as shown in Table 4.5, *GRt* has a larger bias with the observations than *GRz0* (the reference simulation). Thus we assumed that there was no benefit in using time and spatial varying SIT for

MAR at 50 x 50 km resolution.

The reduction of *mzabso* and *mzhyd* (parameters involved in the upper-air scheme), also highlighted interesting features. For example, in contrast with *GRz*, the influence of SIT on temperature expanded above continents for *GRw* simulations (Figure 4.6).

Figures 4.7 and 4.8 show that SIT has an influence on atmospheric circulation. Owing to upper-air relaxation and surface forcing, the strongest changes are observed at 500 hPa, but they are also present at other altitudes. However, the modifications of the wind pattern resulting from changes in SIT are random from one year to the next (Figure 4.9).

In summary, the behaviour of the free set-up of MAR is random and anomalies depend greatly on the selected period (Figure 4.9). This randomness of the atmospheric circulation would have been reduced if we had averaged over a 16 year period but would have been much higher on a daily basis. We assume that these variations from one year to the next are not only due to changes in SIT, but also to a phenomenon called the "butterfly effect" [Meteo France, nd]. According to this effect, a slight difference in the initial conditions can lead a model to yield completely different results. The longer the simulation time, the greater the inconsistencies between the outputs. The butterfly effect is part of every model; for example, GCMs yield an acceptable climate over 30 years, but if we look at a shorter period or a particular year, owing to this effect and depending on the version of the model, the results will be different. So it is clear that SIC and SIT disturb MAR and have an influence on atmospheric circulation, but to what extent has not been established yet.

Chapter 6

Conclusions

Our work investigated the atmospheric influence of SIT over the Arctic between 2000 and 2015. Through the insulation effect of sea ice, the results showed that the inclusion of SIT in MAR has strong impacts on local skin temperature. Effects on a larger scale have also been observed, but they are much weaker than above the Arctic Ocean. Consequently, we believe that coupling MAR with an oceanic model (providing SIT data) is not a priority for improving its model skill at 50 x 50 km of resolution.

6.1 Sources of uncertainty

Climate models are always tainted by a certain degree of uncertainty. Despite their validation, some issues remain and are unavoidable.

6.1.1 Interpolation

The interpolation technique used to convert data on the plane grid of OSTIA and GLO-RYS2v4 to the spherical grid of MAR induced errors. We used the geographical coordinates to identify the pixels that needed to be averaged on the corresponding grid point of MAR. However, given that the spherical pixels had a different shape, this method included errors. The issue encountered here is very common in climatology and will probably require attention in coming years.

6.1.2 Data availability

In contrast to near-surface temperature and sea level pressure observations, precipitation datasets from both ECA&D and NOAA were very poor. In addition, their quality was not guaranteed, given the statistics in Chapter 4. We could expect an underestimation of precipitation from the weather stations. Finally, the underestimation of snowfall is a common issue.

6.2 Perspectives

To complete this last chapter, we include suggestions for further investigation that arise from our research.

6.2.1 Perspective 1

With the accelerated melting of the Arctic ice sheet, it would be interesting to study the implications of sea ice thinning for the climate over the years. We limited ourselves to studying a single period in the past instead of evolution over time. In addition, changes

in circulation patterns have been observed since 2000 [Overland and Wang, 2010]. Therefore, our results could have been slightly different, if we had started the simulations before 2000.

6.2.2 Perspective 2

As mentioned in Chapter 5, owing to the butterfly effect, the influence of SIT and SIC has been established but not quantified. In order to estimate the magnitude of their effect and to remove the butterfly effect from the *GRw* simulations, ensemble runs or Monte Carlo runs could be carried out. Ensemble runs are based on Monte Carlo methods, which are computational algorithms depending on repeated random sampling for the production of numerical results. These methods are useful for simulating systems with many degrees of freedom [Metropolis, 1989].

6.2.3 Perspective 3

The conclusions of this study are valid for MAR at 50 x 50 km resolution. It could be interesting to carry out identical simulations but at higher resolution. Due to small topographical features and less smoothing on extremes, different results could be expected if resolution was increased.

Bibliography

Akperov, M., Mokhov, I., Rinke, A., Handorf, D., and Dethloff, K. (2016). Cyclone activity in the arctic from an ensemble of regional climate models (arctic cordex). In *EGU General Assembly Conference Abstracts*, volume 18, page 243.

Amory, C. (2016). *Érosion éolienne et rugosité de la surface neigeuse en Terre Adélie: observations et approche numérique*. PhD thesis, Université Grenoble Alpes.

Barnes, E. A. and Screen, J. A. (2015). The impact of arctic warming on the midlatitude jet-stream: Can it? has it? will it? *Wiley Interdisciplinary Reviews: Climate Change*, 6(3):277–286.

Bechtold, P., Bazile, E., Guichard, F., Mascart, P., and Richard, E. (2001). A mass-flux convection scheme for regional and global models. *Quarterly Journal of the Royal Meteorological Society*, 127(573):869–886.

Bellprat, O., Kotlarski, S., Lüthi, D., and Schär, C. (2012). Objective calibration of regional climate models. *Journal of Geophysical Research: Atmospheres*, 117(D23).

Benestad, R. E., Hanssen-Bauer, I., and Chen, D. (2008). *Empirical-statistical downscaling*. World Scientific Publishing Company.

Berrisford, P., Dee, D., Poli, P., Brugge, R., Fielding, K., Fuentes, M., Kallberg, P., Kobayashi, S., Uppala, S., and Simmons, A. (2011). The era-interim archive version 2.0, era report series 1, ecmwf, shinfield park. *Reading, UK*, 13177.

Brun, E., David, P., Sudul, M., and Brunot, G. (1992). A numerical model to simulate snow-cover stratigraphy for operational avalanche forecasting. *Journal of Glaciology*, 38(128):13–22.

Cavalieri, D. J., Parkinson, C. L., Gloersen, P., Comiso, J. C., and Zwally, H. J. (1999). Deriving long-term time series of sea ice cover from satellite passive-microwave multisensor data sets. *Journal of Geophysical Research: Oceans*, 104(C7):15803–15814.

Chapman, W. L., Welch, W. J., Bowman, K. P., Sacks, J., and Walsh, J. E. (1994). Arctic sea ice variability: Model sensitivities and a multidecadal simulation. *Journal of Geophysical Research: Oceans*, 99(C1):919–935.

Comiso, J. C. and Nishio, F. (2008). Trends in the sea ice cover using enhanced and compatible amsr-e, ssm/i, and smmr data. *Journal of Geophysical Research: Oceans*, 113(C2).

Comiso, J. C., Parkinson, C. L., Gersten, R., and Stock, L. (2008). Accelerated decline in the arctic sea ice cover. *Geophysical research letters*, 35(1).

Courtier, P., Andersson, E., Heckley, W., Vasiljevic, D., Hamrud, M., Hollingsworth, A., Rabier, F., Fisher, M., and Pailleux, J. (1998). The ecmwf implementation of three-dimensional variational assimilation (3d-var). i: Formulation. *Quarterly Journal of the Royal Meteorological Society*, 124(550):1783–1807.

De Ridder, K. and Gallée, H. (1998). Land surface–induced regional climate change in southern israel. *Journal of applied meteorology*, 37(11):1470–1485.

Dee, D. (2014). ERA-Interim. https://www.ecmwf.int/en/forecasts/datasets/archive-datasets/reanalysis-datasets/era-interim.

Dee, D., Fasullo, J., Shea, D., Walsh, J., and National Center for Atmospheric Research Staff (2016). The climate data guide: Atmospheric reanalysis: Overview and comparison tables. https://climatedataguide.ucar.edu/climate-data/atmospheric-reanalysis-overview-comparison-tables. Online; accessed 20 Mai 2018.

Dee, D. P., Uppala, S., Simmons, A., Berrisford, P., Poli, P., Kobayashi, S., Andrae, U., Balmaseda, M., Balsamo, G., Bauer, d. P., et al. (2011). The era-interim reanalysis: Configuration and performance of the data assimilation system. *Quarterly Journal of the royal meteorological society*, 137(656):553–597.

Delhasse, A. et al. (2017). Résolution spatiale optimale pour modéliser l'inlandsis du groenland.

Deser, C. and Teng, H. (2008). Evolution of arctic sea ice concentration trends and the role of atmospheric circulation forcing, 1979–2007. *Geophysical Research Letters*, 35(2).

Deser, C., Tomas, R., Alexander, M., and Lawrence, D. (2010). The seasonal atmospheric response to projected arctic sea ice loss in the late twenty-first century. *Journal of Climate*, 23(2):333–351.

Deser, C., Walsh, J. E., and Timlin, M. S. (2000). Arctic sea ice variability in the context of recent atmospheric circulation trends. *Journal of Climate*, 13(3):617–633.

Donlon, C. J., Martin, M., Stark, J., Roberts-Jones, J., Fiedler, E., and Wimmer, W. (2012). The operational sea surface temperature and sea ice analysis (ostia) system. *Remote Sensing of Environment*, 116:140–158.

Döscher, R., Vihma, T., and Maksimovich, E. (2014). Recent advances in understanding the arctic climate system state and change from a sea ice perspective: a review. *Atmospheric Chemistry and Physics*, 14(24):13571–13600.

Doutreloup, S., Wyard, C., Belleflamme, A., François, L., Fettweis, X., and Erpicum, M. (2017). Évaluation de la capacité du modèle atmosphérique régional (mar) à simuler la saison des pluies en afrique intertropicale. In *Actes du XXXe colloque de l'Association Internationale de Climatologie: CLIMAT, VILLE ET ENVIRONNEMENT*, pages 389–395.

Duynkerke, P. (1988). Application of the e–ε turbulence closure model to the neutral and stable atmospheric boundary layer. *Journal of the atmospheric sciences*, 45(5):865–880.

Edwards, M. H. and Coakley, B. J. (2003). Scicex investigations of the arctic ocean system. *Chemie der Erde-Geochemistry*, 63(4):281–328.

Ferraro, R. R., Weng, F., Grody, N. C., and Basist, A. (1996). An eight-year (1987–1994) time series of rainfall, clouds, water vapor, snow cover, and sea ice derived from ssm/i measurements. *Bulletin of the American Meteorological Society*, 77(5):891–906.

Fettweis, X. (2006). *Reconstruction of the 1979-2005 Greenland ice sheet surface mass balance using satellite data and the regional climate model MAR*. PhD thesis, Université catholique de Louvain, Louvain-la-neuve, Belgique.

Fettweis, X., Box, J. E., Agosta, C., Amory, C., Kittel, C., Lang, C., van As, D., Machguth, H., and Gallée, H. (2017). Reconstructions of the 1900–2015 greenland ice sheet surface mass balance using the regional climate mar model. *The Cryosphere*, 11(2):1015.

Fouquart, Y. and Bonnel, B. (1980). Computations of solar heating of the earth's atmosphere- a new parameterization. *Beitraege zur Physik der Atmosphaere*, 53:35–62.

Futura (sd). Modèle climatique. https://www.futura-sciences.com/planete/definitions/climatologie-modele-climatique-12896/. Online; accessed 29 Mai 2018.

Gallée, H. (1995). Simulation of the mesocyclonic activity in the ross sea, antarctica. *Monthly Weather Review*, 123(7):2051–2069.

Gallée, H. and Duynkerke, P. G. (1997). Air-snow interactions and the surface energy and mass balance over the melting zone of west greenland during the greenland ice margin experiment. *Journal of Geophysical Research: Atmospheres*, 102(D12):13813–13824.

Gallée, H., Guyomarc'h, G., and Brun, E. (2001). Impact of snow drift on the antarctic ice sheet surface mass balance: possible sensitivity to snow-surface properties. *Boundary-Layer Meteorology*, 99(1):1–19.

Gallée, H. and Schayes, G. (1994). Development of a three-dimensional meso-γ primitive equation model: katabatic winds simulation in the area of terra nova bay, antarctica. *Monthly Weather Review*, 122(4):671–685.

Garric, G., Parent, L., Greiner, E., Drévillon, M., Hamon, M., Lellouche, J.-M., Régnier, C., Desportes, C., Le Galloudec, O., Bricaud, C., et al. (2017). Performance and quality assessment of the global ocean eddy-permitting physical reanalysis glorys2v4. In *EGU General Assembly Conference Abstracts*, volume 19, page 18776.

Gentemann, C. L., Meissner, T., and Wentz, F. J. (2010). Accuracy of satellite sea surface temperatures at 7 and 11 ghz. *IEEE Transactions on Geoscience and Remote Sensing*, 48(3):1009–1018.

Gerdes, R. (2006). Atmospheric response to changes in arctic sea ice thickness. *Geophysical research letters*, 33(18).

Giorgi, f. (2011). Regional climate modelling: Lecture 1 [powerpoint slides]. http://www.to.isac.cnr.it/aosta_old/aosta2011/LecturesSeminars/giorgi1-2.pdf. Online; accessed 18 June 2018.

Giorgi, F., Hewitson, B., Christensen, J., Hulme, M., Von Storch, H., Whetton, P., Jones, R., Mearns, L., Fu, C., Arritt, R., et al. (2001). Regional climate information—evaluation and projections.

Giorgi, F., Jones, C., Asrar, G. R., et al. (2009). Addressing climate information needs at the regional level: the cordex framework. *World Meteorological Organization (WMO) Bulletin*, 58(3):175.

Haylock, M., Hofstra, N., Klein Tank, A., Klok, E., Jones, P., and New, M. (2008). A european daily high-resolution gridded data set of surface temperature and precipitation for 1950–2006. *Journal of Geophysical Research: Atmospheres*, 113(D20).

Hofstra, N., Haylock, M., New, M., and Jones, P. D. (2009). Testing e-obs european high-resolution gridded data set of daily precipitation and surface temperature. *Journal of Geophysical Research: Atmospheres*, 114(D21).

Hu, A., Rooth, C., Bleck, R., and Deser, C. (2002). Nao influence on sea ice extent in the eurasian coastal region. *Geophysical Research Letters*, 29(22).

Jakobsson, M., Macnab, R., Mayer, L., Anderson, R., Edwards, M., Hatzky, J., Schenke, H. W., and Johnson, P. (2008). An improved bathymetric portrayal of the arctic ocean: Implications for ocean modeling and geological, geophysical and oceanographic analyses. *Geophysical Research Letters*, 35(7).

Kendon, E. J., Jones, R. G., Kjellström, E., and Murphy, J. M. (2010). Using and designing gcm–rcm ensemble regional climate projections. *Journal of Climate*, 23(24):6485–6503.

Kittel, C. et al. (2016). *Bilan de masse en surface à haute résolution au Groenland à l'aide du modèle MAR et d'une technique de régionalisation couplée*. PhD thesis, Université de Liège, Liège, Belgique.

Klein Tank, A., Wijngaard, J., Können, G., Böhm, R., Demarée, G., Gocheva, A., Mileta, M., Pashiardis, S., Hejkrlik, L., Kern-Hansen, C., et al. (2002). Daily dataset of 20th-century surface air temperature and precipitation series for the european climate assessment. *International journal of climatology*, 22(12):1441–1453.

Klok, E. and Klein Tank, A. (2009). Updated and extended european dataset of daily climate observations. *International Journal of Climatology*, 29(8):1182–1191.

Koldunov, N. V., Stammer, D., and Marotzke, J. (2010). Present-day arctic sea ice variability in the coupled echam5/mpi-om model. *Journal of Climate*, 23(10):2520–2543.

Kotlarski, S., Keuler, K., Christensen, O. B., Colette, A., Déqué, M., Gobiet, A., Goergen, K., Jacob, D., Lüthi, D., Van Meijgaard, E., et al. (2014). Regional climate modeling on european scales: a joint standard evaluation of the euro-cordex rcm ensemble. *Geoscientific Model Development*, 7(4):1297–1333.

Krinner, G., Rinke, A., Dethloff, K., and Gorodetskaya, I. V. (2010). Impact of prescribed arctic sea ice thickness in simulations of the present and future climate. *Climate dynamics*, 35(4):619–633.

Kurtz, N., Farrell, S., Studinger, M., Galin, N., Harbeck, J., Lindsay, R., Onana, V., Panzer, B., and Sonntag, J. (2012). Sea ice thickness, freeboard, and snow depth products from operation icebridge airborne data. *The Cryosphere Discussions*, 6:4771–4827.

Kwok, R., Cunningham, G., Zwally, H., and Yi, D. (2007). Ice, cloud, and land elevation satellite (icesat) over arctic sea ice: Retrieval of freeboard. *Journal of Geophysical Research: Oceans*, 112(C12).

Kwok, R. and Rothrock, D. (2009). Decline in arctic sea ice thickness from submarine and icesat records: 1958–2008. *Geophysical Research Letters*, 36(15).

Kwok, R. and Untersteiner, N. (2011). The thinning of arctic sea ice. *Phys. Today*, 64(4):36–41.

Lang, A., Yang, S., and Kaas, E. (2017). Sea ice thickness and recent arctic warming. *Geophysical Research Letters*, 44(1):409–418.

Lang, C. (2011). *Modeling of the surface mass balance in Svalbard with the regional climate model MAR over 1958-2010*. PhD thesis, Université de Liège, Liège, Belgique.

Lang, C. (2012). *Modélisation du bilan de masse en surface du Svalbard avec le modèle régional MAR entre 1958 et 2010*. PhD thesis, Université de Liège, Liège, Belgique.

Laxon, S. W., Giles, K. A., Ridout, A. L., Wingham, D. J., Willatt, R., Cullen, R., Kwok, R., Schweiger, A., Zhang, J., Haas, C., et al. (2013). Cryosat-2 estimates of arctic sea ice thickness and volume. *Geophysical Research Letters*, 40(4):732–737.

Lefebre, F., Gallée, H., van Ypersele, J.-P., and Greuell, W. (2003). Modeling of snow and ice melt at eth camp (west greenland): a study of surface albedo. *Journal of Geophysical Research: Atmospheres*, 108(D8).

Lindsay, R. and Schweiger, A. (2015). Arctic sea ice thickness loss determined using subsurface, aircraft, and satellite observations. *The Cryosphere*, 9(1):269–283.

Lindsay, R., Zhang, J., Schweiger, A., Steele, M., and Stern, H. (2009). Arctic sea ice retreat in 2007 follows thinning trend. *Journal of Climate*, 22(1):165–176.

Lott, J. N. and Baldwin, R. (2001). 6.2 the fcc integrated surface hourly database, a new resource of global climate data.

Marbaix, P., Gallée, H., Brasseur, O., and van Ypersele, J.-P. (2003). Lateral boundary conditions in regional climate models: a detailed study of the relaxation procedure. *Monthly weather review*, 131(3):461–479.

Maslanik, J., Fowler, C., Stroeve, J., Drobot, S., Zwally, J., Yi, D., and Emery, W. (2007). A younger, thinner arctic ice cover: Increased potential for rapid, extensive sea-ice loss. *Geophysical Research Letters*, 34(24).

Meteo France (nd). Glossaire. Online; accessed 21 July 2018.

Metropolis, N. (1989). Monte carlo method. *From Cardinals to Chaos: Reflection on the Life and Legacy of Stanislaw Ulam*, page 125.

Morcrette, J.-J. (2002). The surface downward longwave radiation in the ecmwf forecast system. *Journal of climate*, 15(14):1875–1892.

Murphy, J. M., Booth, B. B., Collins, M., Harris, G. R., Sexton, D. M., and Webb, M. J. (2007). A methodology for probabilistic predictions of regional climate change from perturbed physics ensembles. *Philosophical Transactions of the Royal Society of London A: Mathematical, Physical and Engineering Sciences*, 365(1857):1993–2028.

Nael, L. (2006). NNDC Climate Data Online, Global Summary Of the Day. https://www7.ncdc.noaa.gov/CDO/GSOD_DESC.txt. Online; accessed 29 Mai 2018.

Navari, M., Margulis, S., Bateni, S., Tedesco, M., Alexander, P., and Fettweis, X. (2016). Feasibility of improving a priori regional climate model estimates of greenland ice sheet surface mass loss through assimilation of measured ice surface temperatures. *The Cryosphere*, 10(1):103–120.

Noel, B., Fettweis, X., Van De Berg, W., Van Den Broeke, M., and Erpicum, M. (2014). Sensitivity of greenland ice sheet surface mass balance to perturbations in sea surface temperature and sea ice cover: a study with the regional climate model mar. *Cryosphere (The)*, 8:1871–1883.

NSIDC (2017). October | 2017 | arctic sea ice news and analysis. https://nsidc.org/arcticseaicenews/2017/10/. Online; accessed 1 August 2018.

Ogi, M., Yamazaki, K., and Wallace, J. M. (2010). Influence of winter and summer surface wind anomalies on summer arctic sea ice extent. *Geophysical Research Letters*, 37(7).

Omrani, H., Drobinski, P., and Dubos, T. (2012). Spectral nudging in regional climate modelling: how strongly should we nudge? *Quarterly Journal of the Royal Meteorological Society*, 138(668):1808–1813.

Overland, J. E., Francis, J. A., Hanna, E., and Wang, M. (2012). The recent shift in early summer arctic atmospheric circulation. *Geophysical Research Letters*, 39(19).

Overland, J. E. and Wang, M. (2010). Large-scale atmospheric circulation changes are associated with the recent loss of arctic sea ice. *Tellus A*, 62(1):1–9.

O'Carroll, A. G., Saunders, R. W., and Watts, J. G. (2006). The measurement of the sea surface temperature by satellites from 1991 to 2005. *Journal of Atmospheric and Oceanic Technology*, 23(11):1573–1582.

Parkinson, C. L., Cavalieri, D. J., Gloersen, P., Zwally, H. J., and Comiso, J. C. (1999). Arctic sea ice extents, areas, and trends, 1978–1996. *Journal of Geophysical Research: Oceans*, 104(C9):20837–20856.

Peacock, N. R. and Laxon, S. W. (2004). Sea surface height determination in the arctic ocean from ers altimetry. *Journal of Geophysical Research: Oceans*, 109(C7).

Perovich, D. K., Light, B., Eicken, H., Jones, K. F., Runciman, K., and Nghiem, S. V. (2007). Increasing solar heating of the arctic ocean and adjacent seas, 1979–2005: Attribution and role in the ice-albedo feedback. *Geophysical Research Letters*, 34(19).

Pfaffling, A., Haas, C., and Reid, J. E. (2007). Direct helicopter em—sea-ice thickness inversion assessed with synthetic and field data. *Geophysics*, 72(4):F127–F137.

Pithan, F. and Mauritsen, T. (2014). Arctic amplification dominated by temperature feedbacks in contemporary climate models. *Nature Geoscience*, 7(3):181–184.

Pohl, B. and Crétat, J. (2014). On the use of nudging techniques for regional climate modeling: application for tropical convection. *Climate dynamics*, 43(5-6):1693–1714.

Polyakov, I. V. and Johnson, M. A. (2000). Arctic decadal and interdecadal variability. *Geophysical Research Letters*, 27(24):4097–4100.

Quadrelli, R. and Wallace, J. M. (2004). A simplified linear framework for interpreting patterns of northern hemisphere wintertime climate variability. *Journal of Climate*, 17(19):3728–3744.

Rae, J., Aðalgeirsdóttir, G., Edwards, T., Fettweis, X., Gregory, J., Hewitt, H., Lowe, J., Lucas-Picher, P., Mottram, R., Payne, A., et al. (2012). Greenland ice sheet surface mass balance: evaluating simulations and making projections with regional climate models. *The Cryosphere*, 6:1275–1294.

Rayner, N., Brohan, P., Parker, D., Folland, C., Kennedy, J., Vanicek, M., Ansell, T., and Tett, S. (2006). Improved analyses of changes and uncertainties in sea surface temperature measured in situ since the mid-nineteenth century: The hadsst2 dataset. *Journal of Climate*, 19(3):446–469.

Reanalyses.org (2010). Advancing reanalysis. http://reanalyses.org/.

Reijmer, C., Van den Broeke, M., Fettweis, X., Ettema, J., and Stap, L. (2012). Refreezing on the greenland ice sheet: a comparison of parameterizations. *The Cryosphere*, 6:743–762.

Ridder, K. D. and Schayes, G. (1997). The iagl land surface model. *Journal of applied meteorology*, 36(2):167–182.

Rignot, E., Velicogna, I., van den Broeke, M. R., Monaghan, A., and Lenaerts, J. T. (2011). Acceleration of the contribution of the greenland and antarctic ice sheets to sea level rise. *Geophysical Research Letters*, 38(5).

Rinke, A., Maslowski, W., Dethloff, K., and Clement, J. (2006). Influence of sea ice on the atmosphere: A study with an arctic atmospheric regional climate model. *Journal of Geophysical Research: Atmospheres*, 111(D16).

Roberts-Jones, J., Fiedler, E. K., and Martin, M. J. (2012). Daily, global, high-resolution sst and sea ice reanalysis for 1985–2007 using the ostia system. *Journal of Climate*, 25(18):6215–6232.

Rockel, B. (2015). The regional downscaling approach: a brief history and recent advances. *Current Climate Change Reports*, 1(1):22–29.

Romanov, I. (1995). Atlas of ice and snow of the arctic basin and siberian shelf seas, translated from russian by a. *Tunik, Backbone, Paramus, NJ*.

Rothrock, D., Percival, D., and Wensnahan, M. (2008). The decline in arctic sea-ice thickness: Separating the spatial, annual, and interannual variability in a quarter century of submarine data. *Journal of Geophysical Research: Oceans*, 113(C5).

Rothrock, D. A., Yu, Y., and Maykut, G. A. (1999). Thinning of the arctic sea-ice cover. *Geophysical Research Letters*, 26(23):3469–3472.

Schneider, S. H. and Dickinson, R. E. (1974). Climate modeling. *Reviews of Geophysics*, 12(3):447–493.

Scholzen, C. (2015). *Study of the recent disappearance of a tropical glacier in the Bolivian Andes with the help of the high resolution regional climate model MAR*. PhD thesis, Université de Liège, Liège, Belgique.

Screen, J. A. and Simmonds, I. (2010). The central role of diminishing sea ice in recent arctic temperature amplification. *Nature*, 464(7293):1334.

Screen, J. A., Simmonds, I., Deser, C., and Tomas, R. (2013). The atmospheric response to three decades of observed arctic sea ice loss. *Journal of Climate*, 26(4):1230–1248.

Serreze, M. C., Barrett, A. P., Slater, A. G., Steele, M., Zhang, J., and Trenberth, K. E. (2007a). The large-scale energy budget of the arctic. *Journal of Geophysical Research: Atmospheres*, 112(D11).

Serreze, M. C. and Barry, R. G. (2011). Processes and impacts of arctic amplification: A research synthesis. *Global and Planetary Change*, 77(1):85–96.

Serreze, M. C., Holland, M. M., and Stroeve, J. (2007b). Perspectives on the arctic's shrinking sea-ice cover. *science*, 315(5818):1533–1536.

Smith, A., Lott, N., and Vose, R. (2011). The integrated surface database: Recent developments and partnerships. *Bulletin of the American Meteorological Society*, 92(6):704–708.

Stark, J. D., Donlon, C. J., Martin, M. J., and McCulloch, M. E. (2007). Ostia: An operational, high resolution, real time, global sea surface temperature analysis system. In *Oceans 2007-Europe*, pages 1–4. IEEE.

Steele, M. and Flato, G. M. (2000). Sea ice growth, melt, and modeling: A survey. In *The freshwater budget of the Arctic Ocean*, pages 549–587. Springer.

Stroeve, J., Holland, M. M., Meier, W., Scambos, T., and Serreze, M. (2007). Arctic sea ice decline: Faster than forecast. *Geophysical research letters*, 34(9).

Stroeve, J., Serreze, M., Drobot, S., Gearheard, S., Holland, M., Maslanik, J., Meier, W., and Scambos, T. (2008). Arctic sea ice extent plummets in 2007. *Eos, Transactions American Geophysical Union*, 89(2):13–14.

Stroeve, J. C., Kattsov, V., Barrett, A., Serreze, M., Pavlova, T., Holland, M., and Meier, W. N. (2012a). Trends in arctic sea ice extent from cmip5, cmip3 and observations. *Geophysical Research Letters*, 39(16).

Stroeve, J. C., Serreze, M. C., Holland, M. M., Kay, J. E., Malanik, J., and Barrett, A. P. (2012b). The arctic's rapidly shrinking sea ice cover: a research synthesis. *Climatic Change*, 110(3-4):1005–1027.

Tedesco, M., Doherty, S., Fettweis, X., Alexander, P., Jeyaratnam, J., and Stroeve, J. (2016). The darkening of the greenland ice sheet: trends, drivers, and projections (1981–2100). *Cryosphere (The)*, 10:477–496.

van de Berg, W. J. and Medley, B. (2016). Brief communication: Upper-air relaxation in racmo2 significantly improves modelled interannual surface mass balance variability in antarctica. *The Cryosphere*, 10(1):459–463.

Vernon, C. L., Bamber, J., Box, J., Van den Broeke, M., Fettweis, X., Hanna, E., and Huybrechts, P. (2013). Surface mass balance model intercomparison for the greenland ice sheet. *The Cryosphere*, 7:599–614.

Vinnikov, K. Y., Robock, A., Stouffer, R. J., Walsh, J. E., Parkinson, C. L., Cavalieri, D. J., Mitchell, J. F., Garrett, D., and Zakharov, V. F. (1999). Global warming and northern hemisphere sea ice extent. *Science*, 286(5446):1934–1937.

Wang, J., Zhang, J., Watanabe, E., Ikeda, M., Mizobata, K., Walsh, J. E., Bai, X., and Wu, B. (2009). Is the dipole anomaly a major driver to record lows in arctic summer sea ice extent? *Geophysical Research Letters*, 36(5).

Wang, Y., Leung, L. R., McGREGOR, J. L., Lee, D.-K., Wang, W.-C., Ding, Y., and Kimura, F. (2004). Regional climate modeling: progress, challenges, and prospects. *Journal of the Meteorological Society of Japan. Ser. II*, 82(6):1599–1628.

Watanabe, E., Wang, J., Sumi, A., and Hasumi, H. (2006). Arctic dipole anomaly and its contribution to sea ice export from the arctic ocean in the 20th century. *Geophysical research letters*, 33(23).

WCRP (2015). Criteria for selecting and updating cordex domains. `http://cordex.org.preview.binero.se/wp-content/uploads/2012/11/Domain_Criteria_Document_FINAL.pdf`. Online; accessed 18 June 2018.

WCRP CORDEX (2018). Region 11: Arctic. `http://www.cordex.org/domains/region-11-arctic/`. Online; accessed 18 August 2018.

W.M.O. (2016). World weather watch. `https://www.wmo.int/pages/prog/www/index_en.html`. Online; accessed 20 Mai 2018.

Worby, A. P., Geiger, C. A., Paget, M. J., Van Woert, M. L., Ackley, S. F., and DeLiberty, T. L. (2008). Thickness distribution of antarctic sea ice. *Journal of Geophysical Research: Oceans*, 113(C5).

Wyard, C., Fettweis, X., and Erpicum, M. (2015). Etude de l'évolution de l'enneigement dans les hautes fagnes (belgique) au cours des cinquante dernières années à l'aide du modèle climatique régional mar. In *Actes du XXVIIIe colloque annuel de l'Association Internationale de Climatologie: Modélisations et variabilités*. ULg.

Zhang, Y. and Hunke, E. C. (2001). Recent arctic change simulated with a coupled ice-ocean model. *Journal of Geophysical Research: Oceans*, 106(C3):4369–4390.

Zhong, Z., Wang, X., Lu, W., and Hu, Y. (2010). Further study on the effect of buffer zone size on regional climate modeling. *Climate dynamics*, 35(6):1027–1038.